

**Geochemical Investigations into a Miocene/Pliocene Tephra Which May Constrain the
Timing of Cervidae in North America**

A Senior Honors Thesis Presented to the Faculty of the
Department of Earth and Atmospheric Sciences

University of Houston

In Partial Fulfillment of the Requirements for the Degree of Bachelor of Science

By

Shawn A. Fields

May 2023

**Geochemical Investigations into a Miocene/Pliocene Tephra Which May Constrain the
Timing of Cervidae in North America**

Shawn A. Fields

APPROVED:

Dr. Tom Lapen, Chair

Dr. Peter Copeland

Nick Zentner

Dr. Dan E. Wells, Dean
College of Natural Sciences and Mathematics

Acknowledgments

My special thanks go to Dr. Tom Lapen for taking me onto this project and for his guidance and support throughout the project. My sincerest appreciation goes to Minako Righter for teaching me the basics of working in the lab and for assisting me with the lab work required to complete the project. I could not have been able to complete this project without her assistance. I would also like to thank my friend Ruby Patterson, PhD Candidate at University of Houston, for encouraging me to seek out research opportunities. I truly appreciate Bianca Rombado who has supported me throughout my journey at the University of Houston and for her constant encouragement. Last, but not least, my deepest thanks go to my friends and family who have supported me throughout my journey.

**Geochemical Investigations into a Miocene/Pliocene Tephra Which May Constrain the
Timing of Cervidae in North America**

An Abstract of a Senior Honors Thesis
Presented to the Faculty of the Department
of Earth and Atmospheric Sciences

University of Houston

In Partial Fulfillment of the Requirements for the Degree of Bachelor of Science

By
Shawn A. Fields
May 2023

Craigs Hill is an outcrop of Pliocene to present deposits located in Ellensburg, Washington, that sits on a resistant portion of the Miocene Ellensburg formation. Within Craigs Hill, there has been a recent discovery of a paleosol containing cervid fossils of the genus *Bretzia*. An aliquot of hornblende crystals from a tephra unit directly above the paleosol has been dated to 4.9 ± 0.1 Ma by $^{40}\text{Ar}/^{39}\text{Ar}$ analyses, indicating the fossils could represent some of the oldest Cervidae occurrences in North America.

Using LA-ICP-MS, 47 zircon grains from the same tephra unit overlying the paleosol were analyzed for their U-Th-Pb isotopic compositions. The youngest cluster of zircons define a Tera-Wasserburg lower intercept age of 4.15 ± 0.10 Ma (2σ ; $n=18$). The U-Pb age data of zircon also show that the tephra unit is not a simple air-fall tephra but was reworked and contains detrital zircons ranging from Pliocene to Proterozoic. The approximately 800,000-year discrepancy in the zircon and hornblende dates could be due to excess argon in the hornblende and/or older detrital hornblende grains included in the analyzed aliquot. The new U-Pb age for the tephra suggests this outcrop may not contain a new early occurrence of *Bretzia*.

The Nd isotopic composition of the tephra magma source was determined from ~150 phosphate minerals that were digested, chemically processed, and analyzed by MC-ICP-MS. The Nd isotopic composition, referenced against present-day CHUR, yielded an ϵ_{Nd} value of $+6.83 \pm 0.20$. The ϵ_{Nd} values from rocks derived from the Yellowstone and Mt. Adams volcanic centers are between -24.8 to +4.2 and between +5.35 to +7.24, respectively. The ϵ_{Nd} value of +6.83 from this study is consistent with values found in the Mount Adams volcanic field. We conclude that the tephra layer of Craigs Hill is most likely related to a Cascade Arc magmatic event at 4.15 ± 0.10 Ma.

Table of Contents

Cover Page.....	<i>i</i>
Signature Page.....	<i>ii</i>
Acknowledgments.....	<i>iii</i>
Abstract Cover Page.....	<i>iv</i>
Abstract.....	<i>v</i>
Table of Contents.....	<i>vi</i>
List of Figures.....	<i>vii</i>
List of Tables.....	<i>viii</i>
Chapter I: Introduction.....	<i>1</i>
Section I.A. Geologic Setting:.....	<i>1</i>
Section I.B. Argon Dating and Potential Issues.....	<i>6</i>
Section I.C. LA-ICP-MS U-Pb Zircon Dating.....	<i>10</i>
Section I.D. Potential Issues with U-Pb Dating.....	<i>11</i>
Section I.E. Potential Sources of Craigs Hill Tephra.....	<i>13</i>
Chapter II: Methods.....	<i>14</i>
Section II.A. Extraction of Heavy Minerals.....	<i>14</i>
Section II.B. In Situ U-Th-Pb Isotope Analysis of Zircon.....	<i>17</i>
Section II.C. Neodymium Isotope Analysis.....	<i>18</i>
Chapter III: Results.....	<i>20</i>
Section III.A. LA-ICP-MS of Zircon.....	<i>20</i>
Section III.B. MC-ICP-MS of Phosphate Minerals.....	<i>28</i>
Chapter IV: Discussion.....	<i>30</i>
Section IV.A. Questions Surrounding the Age of the Tephra Layer.....	<i>30</i>
Section IV.A.i. Determining a Maximum Age of Deposition.....	<i>32</i>
Section IV.A.ii. Could Excess Argon Explain the Different Ages?.....	<i>33</i>
Section IV.A.iii. Detrital Hornblende Possibly Included in Analysis.....	<i>35</i>
Section IV.B. Detrital Zircons Within the Tephra.....	<i>36</i>
Section IV.C. Swakane Gneiss Zircon Signatures Found in Craigs Hill?.....	<i>36</i>
Section IV.D. Possible Source of ~90Ma Zircon Grains.....	<i>37</i>
Section IV.E. Phosphate Nd Isotopic Composition.....	<i>39</i>
Section IV.F. Implications for the timing of Cervidae in North America.....	<i>41</i>
Chapter V: Conclusion.....	<i>43</i>
Appendices.....	<i>44</i>
Bibliography.....	<i>50</i>

List of Figures

Figure 1: Generalized stratigraphic column showing the Ellensburg Formation.....	2
Figure 2: Stratigraphic Column of Craigs Hill.....	4
Figure 3: Wetherill concordia diagram for all zircon grains analyzed.....	21
Figure 4: Wetherill concordia diagram for all zircon grains aged under 110Ma	22
Figure 5: Terra-Wasserburg concordia diagram for all grains approximately 4 Ma.....	23
Figure 6: Tera-Wasserburg concordia diagram for a single 6.5 Ma zircon grain.....	24
Figure 7: Weighted mean age plot for zircon grain approximately 6.5 Ma	25
Figure 8: Tera-Wasserburg Concordia Diagram showing grains approximately 70-80 Ma.	26
Figure 9: Tera-Wasserburg concordia diagram for 4 zircon grains approximately 90Ma.....	27
Figure 10: Weighted mean age plot for zircon grains approximately 90Ma.....	28
Figure 11: Equation used for calculating ϵ Nd	29
Figure 12: Updated stratigraphic column of Craigs Hill.....	31
Figure 13: Argon release spectra data from Lamb, (1997).....	34
Figure 14: Graph comparing ϵ Nd values of Craigs Hill tephra to three other samples.....	40

List of Tables

Table 1: MC-ICP-MS data for Craigs Hill Tephra.....	29
Table 2: Argon release data from Lamb, (1997).....	44
Table 3: Zircon LA-ICP-MS isotope data	45
Table 4: Zircon LA-ICP-MS apparent age data	47
Table 5: Zircon LA-ICP-MS data included in youngest cluster of grains	48
Table 6: Zircon LA-ICP-MS apparent age data included in youngest cluster of grains.....	49

Chapter I: Introduction

Section I.A. Geologic Setting:

The Kittitas Valley in central Washington, USA, is part of the Yakima River Valley. The Yakima River is a tributary of the Columbia River and is named after the local Indigenous Yakama people. The Yakima River is approximately 214 miles long and begins in the highlands of the Cascade Range and flows downstream eastward to the Columbia River. The Kittitas Valley basin is filled with a series of gravels, glacial outwash deposits, till, volcanoclastic sediments, tuff, sandstones, mudstones, lacustrine deposits, and many other sediment types (Waitt, 1979; Smith, 1988). The local geology of the Kittitas Valley has been affected by intense Miocene volcanism and tectonic shortening that produced a series of folds and reverse faults. Much of the Miocene volcanism is recorded in the Ellensburg Formation.

The Ellensburg Formation is a Miocene-Pliocene sedimentary and volcanoclastic package found in central Washington, USA. It is named after the town of Ellensburg, Washington. The Ellensburg Formation is interfingered with and overlies the Columbia River Basalt Group (Smith, 1988). The Columbia River Basalt Group is a Miocene series of flood basalts that were deposited from ~16.7 Ma to 5.5 Ma (Reidel et al., 2013). The Ellensburg Formation is composed of ash fall units, conglomerate, sandstone, mudstone, tuff and pyroclastic flow deposits (Smith, 1988). The Upper Ellensburg Formation generally refers to the sedimentary layers deposited above the Ponomo Member of the Saddle Mountains Basalt Formation which is dated at 11.5 Ma

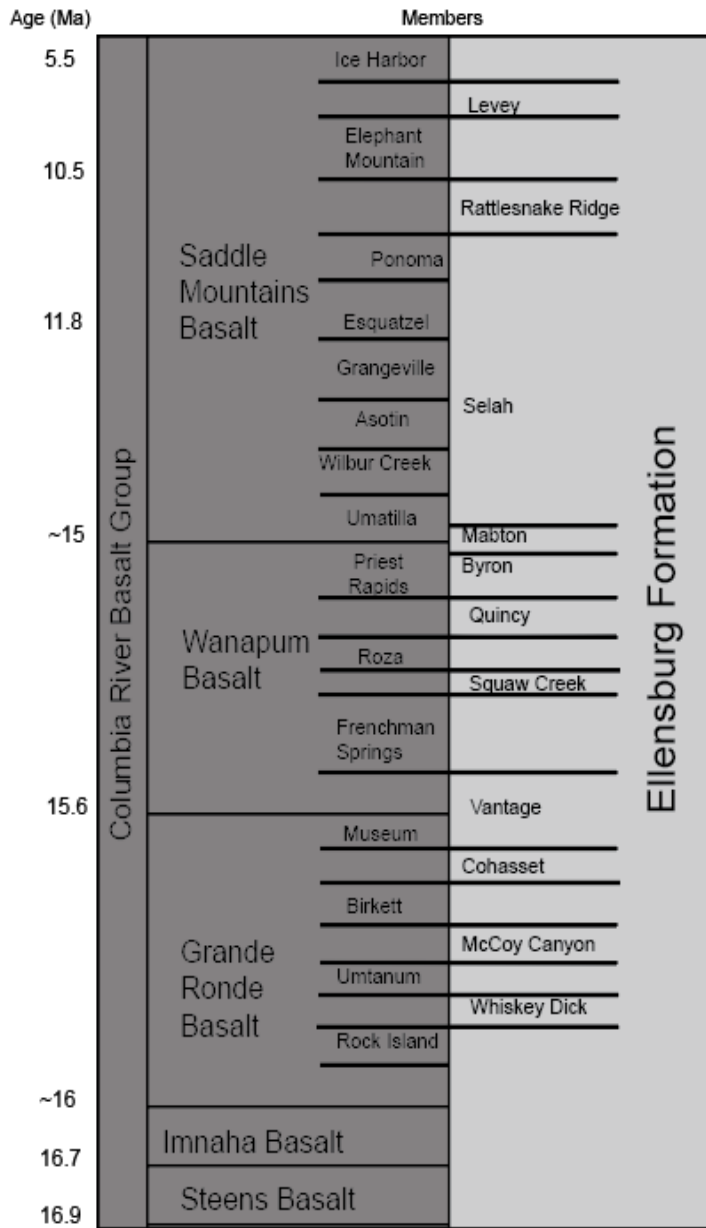


Figure 1: Generalized stratigraphic column showing the Ellensburg Formation intercalated with the Columbia River Basalt Group. Made with data from Emery-Wetherell & Schilter, (2020) and Reidel et al., (2013).

(Smith, 1988). The Upper Ellensburg formation consists of a variety of sediments including fluvial sandstones, mudstones, lahar flows, and conglomerate. Figure 1 shows a generalized stratigraphic column of the Ellensburg Formation. The dark-gray left side of the column represents the various members of Columbia River Basalt Group and the light-gray, right side represents the sedimentary units of the Ellensburg Formation intercalated with the Columbia River Basalt Group.

Craigs Hill is an outcrop which sits on a slope of a resistant portion of the Ellensburg Formation. The

uppermost layer of Craigs Hill is a series of loess and sheet-wash deposits dated as Pleistocene to recent (Lamb, 1997). Below this layer is the Pliocene-aged Thorp Gravel which varies in thickness throughout the Kittitas Valley and is approximately 200 meters

thick at its thickest locations. Zircon fission track dates of air-fall tuff sediments near the top of the gravel layer are 3.7 ± 0.2 Ma (Waitt, 1979). The date of the Upper Ellensburg Formation – Thorp Gravel contact is likely diachronous, but perhaps as old as 4.7 ± 0.2 Ma (Figure 2; Smith, 1988). The Thorp Gravel consists of two facies: mainstream gravel consisting of rounded to subrounded silicic volcanic rocks deposited by the Yakima River (Smith, 1988) and sidestream gravel consisting of subangular clasts of the Grande Ronde Basalt (Smith, 1988; Lamb, 1997). This layer unconformably overlies the Ellensburg Formation.

Craigs Hill is of particular importance because of a recent discovery of a cervid fossil in a paleosol layer immediately below a tephra dated at 4.9 ± 0.1 Ma using $^{40}\text{Ar}/^{39}\text{Ar}$ in hornblende (Lamb, 1997; Emery-Wetherell & Schilter, 2020). This age supported a hypothesis that Cervidae entered North America approximately 5 million years ago (Webb, 2000) and that the fossils on Craigs Hill are some of the oldest cervid fossils found in North America (Emery-Wetherell & Schilter, 2020). Figure 2 shows a stratigraphic column of Craigs Hill and the tephra layer that was $^{40}\text{Ar}/^{39}\text{Ar}$ dated is labeled with a yellow triangle labeled “4.9”. The overbank deposit in which the fragment of cervid jaw with several teeth attached was found is marked with a green triangle labeled “B” (Figure 2).

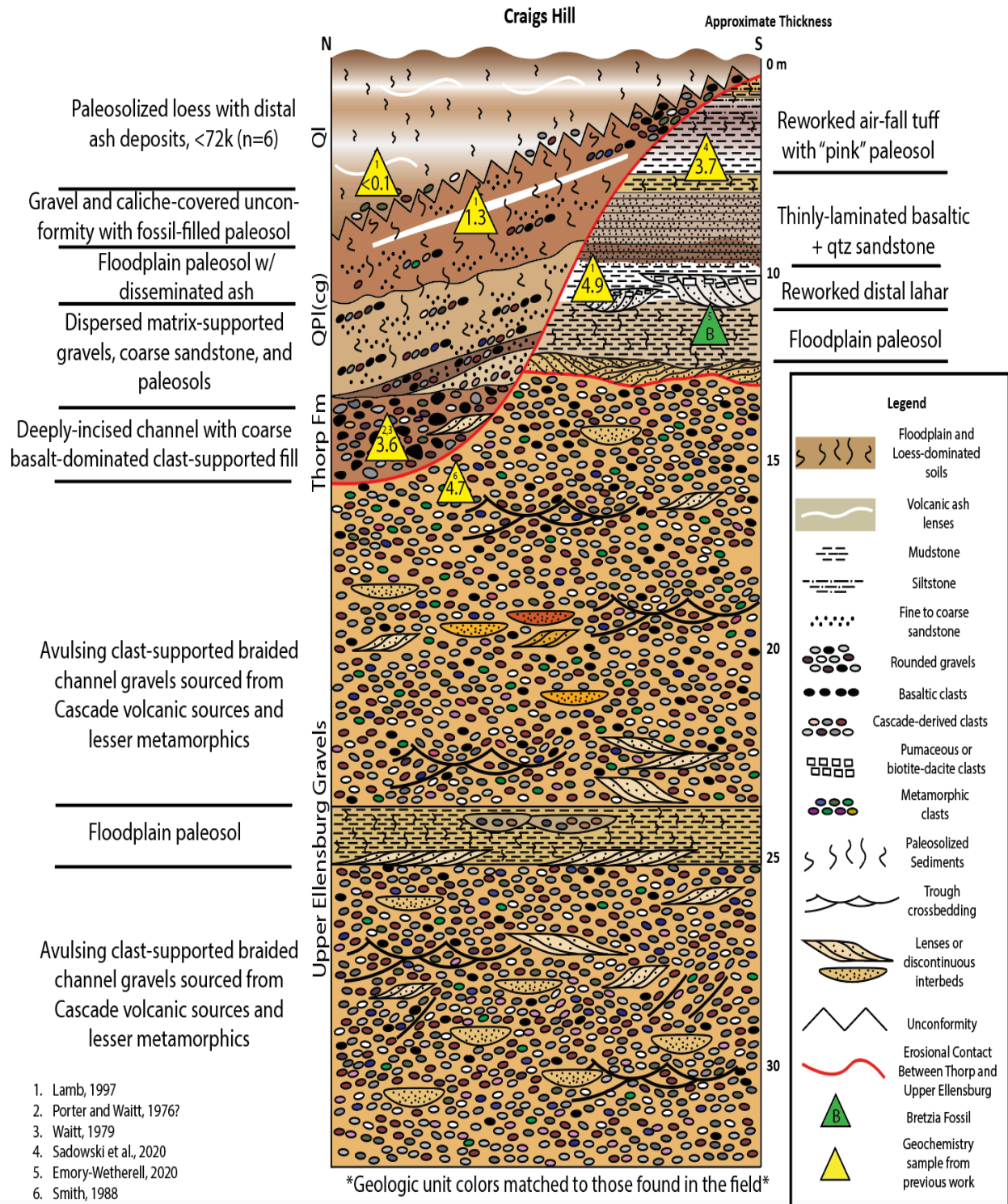


Figure 2: Stratigraphic Column of Craigs Hill. Yellow triangle labeled “4.9” shows the location of the tephra layer dated in Lamb, (1997). Green triangle labeled “B” marks the location of cervid mandible fragments detailed in Emery-Wetherell & Schilter, (2020). Modified from personal communication (Wetherell, 2023)

Past studies of Craigs Hill include dating of the various stratigraphic layers using a variety of dating techniques. The uppermost layer of Pleistocene-Holocene loess and sheet-wash deposits to having been deposited in the last 1.32 ± 0.24 Ma (Waitt, 1979). Fission track dating of the airfall tuffs near the top of the Thorp Gravel range from 3.64 ± 0.74 Ma to 3.70 ± 0.20 Ma (Waitt, 1979). Another study focused on the differentiation of the two gravel facies found within the Thorp Gravel determined widespread basaltic side stream gravel was deposited by streams flowing down from the anticlinal ridges which surround the valley and mainstream gravel deposited from the Yakima River (Waitt, 1979, Smith, 1988). $^{40}\text{Ar}/^{39}\text{Ar}$ dating of hornblende grains within the tephra unit of Craigs Hill performed by the New Mexico Bureau of Mines & Mineral Resources determined an age of 4.9 ± 0.1 Ma which was reported in a thesis studying the stratigraphy of the Kittitas Valley (Lamb, 1997).

We address three main questions in this study:

1. Is the $^{40}\text{Ar}/^{39}\text{Ar}$ derived age of 4.9 ± 0.1 Ma presented in Lamb, (1997) a robust and reliable age of this tephra?
2. Does this tephra form a new upper constraint on the arrival of Cervidae in North America?
3. What is the source of the tephra?
 - a. Is this tephra derived from Cascade Arc magmatism?
 - b. Could this tephra be related to the Yellowstone Hotspot track eruptions?

To investigate the $^{40}\text{Ar}/^{39}\text{Ar}$ derived age, we look at using an alternative method to date the tephra which will either confirm the age of 4.9 ± 0.1 Ma or provide a new age

for the tephra. We use laser ablation inductively coupled mass spectrometry (LA-ICP-MS) of zircon grains to date the tephra using the U-Pb system. Uranium-Pb dating of zircon has the potential for more accurate age determinations for such young units than $^{40}\text{Ar}/^{39}\text{Ar}$ dating of hornblende, which has a relatively low K content. By using a second dating method to test the age of the tephra, we are also able to determine if this tephra forms an early constraint on the arrival of Cervidae in North America.

To determine a valid source of the Craigs Hill tephra, Nd isotopic compositions of the Craigs Hill tephra are compared to data from Yellowstone rhyolite ash fall tuffs (Nash et al., 2005), samples of the Kilgore Tuff of the Heise volcanic field (Watts et al., 2011), and the Quaternary Mount Adams volcanic field of the Cascade Arc (Jicha et al., 2009). The Nd isotopic compositions of phosphate are used to assess whether the volcanic source is the Cascade arc or from an intraplate source such as the Yellowstone hotspot.

Section I.B. Argon Dating and Potential Issues

The $^{40}\text{Ar}/^{39}\text{Ar}$ radiogenic dating technique is a derivative of the K-Ar dating technique. This dating technique is based on the decay of ^{40}K into ^{40}Ar (Kelley, 2002). The ^{39}Ar nuclide is created by irradiating the sample with neutrons in a nuclear reactor (Schaen et al., 2021). Argon dating techniques are extremely versatile and widely used. The technique depends on the assumption that all ^{40}Ar in the sample is the result of in situ decay of ^{40}K (Kelley, 2002). The $^{40}\text{Ar}/^{39}\text{Ar}$ dates represent the time elapsed since a sample became closed to K mobility and ^{40}Ar loss (Schaen et al., 2021). The $^{40}\text{Ar}/^{39}\text{Ar}$ date of unaltered, rapidly cooled volcanic rocks can be interpreted as the eruption age.

There are also applications of $^{40}\text{Ar}/^{39}\text{Ar}$ dating to metamorphic samples and sedimentary samples. In metamorphic samples, the $^{40}\text{Ar}/^{39}\text{Ar}$ date often represents the cooling age. In sedimentary rocks, $^{40}\text{Ar}/^{39}\text{Ar}$ ages can in some cases represent the date of low temperature chemical reactions (Schaen et al., 2021).

Argon is an inert incompatible trace element in solids and preferentially remains in the fluid phase of solid/liquid systems. The strong incompatibility of argon is primary cause of argon dating techniques yielding true radiogenic ages (Kelley, 2002). This incompatibility also leads to the assumption any Ar found within the mineral structure is due to radioactive decay of potassium, not Ar inherited from the surroundings.

Excess argon occurs when argon is trapped within the sample or mineral grains being examined. Even though argon is incompatible within the crystal structure of most minerals, minor quantities of non-radiogenic argon can be detected in crystal lattices (Kelley, 2002; Schaen et al., 2021). Fluid inclusions and melt inclusions are common sources of excess argon. Low potassium rocks and minerals such as plagioclases and amphiboles are commonly associated with excess argon (Kelley, 2002). The levels of excess argon within melt inclusions are dependent on the argon levels in the magma from which they formed. Melt inclusions incorporated from magma which contains excess argon have been shown to contain up to 100 times more argon than the minerals which crystalized from the same melt (Kelley, 2002). Excess argon concentration levels in fluid inclusions could be as much as 10,000 times higher than the mineral structure (Kelley, 2002). Melt inclusions are commonly found in minerals used to date volcanic rocks.

Incrementally heating low potassium rocks and minerals such as amphiboles and clinopyroxenes often results in saddle-shaped argon release spectra (Kelley, 2002). Initial heating of the sample at low temperatures breaks down fluid inclusions within the sample which results in the older initial ages commonly shown in the release spectra (Kelley, 2002). This initially older apparent age can also be a result of outgassing of potassium rich alteration phases (Schaen et al., 2021). As temperature increases, the argon release decreases until it approaches the 'true age' of the sample. The argon release then begins to exhibit steadily older ages until the end of the analysis. This can be caused by the release of high temperature excess argon (Schaen et al., 2021). The 'true age' of the sample is seen in the plateau of the saddle shape.

While potassium-argon and argon-argon dating are reliable techniques, there are known occurrences of argon dating which have resulted in a significantly older age. The age of a volcanic bomb sample from the September 23rd, 1963, eruption of Mt. Stromboli was determined to be 2.4 ± 2 Ma using K-Ar dating (Krummenacher, 1970). A sample from the 1959 eruption of Kilauea in Hawaii was dated at 8.5 ± 6.8 Ma using K-Ar techniques (Krummenacher, 1970). Anorthoclase sample from the 1984 eruption of Mt. Erebus, Antarctica, was found to be 0.64 ± 0.03 Ma (Esser et al., 1997).

As stated above, dates produced via argon dating techniques are reliant on the assumption that all ^{40}Ar within a sample is the product of ^{40}K decay. Excess argon present within a volcanic rock or mineral must have not completely degassed during eruption and subsequent cooling (Snelling, 1998). The excess argon phenomena have been reproduced in controlled lab experiments. One experiment designed to study the solubility of argon in synthetic basalt melts and minerals at 1300 °C at 1 atm in an

argon-containing gas stream found olivine produced from this melt had 0.34 ppm ^{40}Ar (Broadhurst et al., 1990). This study determined argon solubility was “surprisingly high” and found argon was held within minerals in lattice vacancy defects (Broadhurst et al., 1990).

Recent guidelines are set to help identify erroneous ages focus on a stricter definition of the argon release plateau (e.g., Schaen et al., 2021). In the past, incremental heating of volcanic samples during ^{40}Ar dating involved as few as 5-10 heat increments which could result in an inaccurate plateau. However, it has been suggested $^{40}\text{Ar}/^{39}\text{Ar}$ dating techniques on volcanic rocks require between 15-40 heat increments (Schaen et al., 2021). A more rigid definition of an argon release plateau is required to accurately determine the age of volcanic samples (Schaen et al., 2021). As defined in Schaen et al. (2021), the three modern requirements of an argon plateau are:

1. the plateau must consist of at least 5 or more consecutive steps that comprise at least 50% of the ^{39}Ar released,
2. it must not have a slope and
3. it must have an isochron regressed through all the plateau steps with an initial $^{40}\text{Ar}/^{36}\text{Ar}$ ratio that is indistinguishable from the atmospheric value with a 95% confidence level for terrestrial samples.

Most age spectra derived from incremental heating processes show some level of complexity and may not fit the rigid plateau definition as described above (Schaen et al., 2021). Release spectra that do not sufficiently fulfill these guidelines may still contain geologically useful information but, the age generated from these spectra should be discussed with a wider range of dates or used with caution (Schaen et al., 2021).

Section I.C. LA-ICP-MS U-Pb Zircon Dating

Uranium-lead (U-Pb) dating is a radiogenic dating technique used to determine the age of geologic materials. U-Pb dating is based on the decay of uranium to lead. This method uses two uranium decay chains: ^{238}U decays to ^{206}Pb and ^{235}U decays to ^{207}Pb . Uranium-238 has a half-life of 4.468 billion years and uranium-235 has a half-life of 710 million years. In U and Th-bearing minerals, radiogenic lead isotopes (^{206}Pb , ^{207}Pb , ^{208}Pb) will accumulate over time due to decay of uranium and thorium (Andersen, 2002). Dating minerals using this method focuses on measuring the relative abundances of radiogenic lead isotopes and correcting proportionally to their relative abundances in common lead (Andersen, 2002). Measurements of isotopes are commonly done by laser ablation inductively coupled mass spectrometry (LA-ICP-MS), secondary ion mass spectrometry (SIMS) or thermal ionization mass spectrometry (TIMS). LA-ICP-MS is one of the most popular tools for U-Pb geochronological studies because of its low cost, high throughput, and robust results (e.g., Shaulis et al., 2010). This method of radiogenic dating can be applied to a variety of uranium bearing minerals such as zircon, monazite, titanite, rutile, baddeleyite, or apatite (e.g., Chew et al., 2019).

There are several methods to determine the age of a mineral using the U-Pb system. Tera-Wasserburg concordia diagrams plot measured $^{238}\text{U}/^{206}\text{Pb}$ against measured $^{207}\text{Pb}/^{206}\text{Pb}$ ratios. This method is especially suited for dating young samples and can provide a robust model for correcting the effects of common Pb because the radiogenic-common Pb mixing line is nearly orthogonal to concordia for young (< 200

Ma) samples. Another approach to plotting U-Pb data is the Wetherill diagram where the $^{207}\text{Pb}/^{235}\text{U}$ and $^{206}\text{Pb}/^{238}\text{U}$ ratios are plotted. This method is most useful for portraying older grains (e.g., > 200 Ma) and those older grains with Pb loss and/or inherited cores.

Zircon is widely known as an ideal mineral for U-Pb dating for several reasons. Zircon is a very durable mineral which is difficult to destroy in nature and is difficult to dissolve in the laboratory (Parrish & Noble, 2003). The difficulty to dissolve zircon in the laboratory is useful to researchers because it allows them to dissolve most of the other material and be left with only grains of zircon and some Fe-Cr oxides. Zircon crystals are capable of being transported vast distances from their source region and are found preserved in sedimentary rocks. (Parrish & Noble, 2003). The primary reason zircon is widely targeted for radiogenic U-Pb dating is zircon incorporates a moderate amount of uranium and thorium but rejects common lead during crystallization (Parrish & Noble, 2003; Chew et al., 2019). This leads to the assumption any radiogenic lead found within a zircon crystal, must be the product of uranium decay and that any measured common (non-radiogenic) Pb is derived from contamination along cracks and/or mineral/melt inclusions. This makes dating zircon grains via uranium decay a remarkably accurate tool for geochronological studies.

Section I.D. Potential Issues with U-Pb Dating

While U-Pb dating is a reliable and proven method for dating geologic materials, there are several potential issues which could affect the accuracy of the date such as Pb mobility, common Pb contamination, or inheritance of older cores. Pb mobility refers

to Pb migration within the mineral lattice (Spencer et al., 2016). Common Pb refers to the presence of non-radiogenic Pb (as detected from the ^{204}Pb abundance) measured within a mineral. Inheritance of older cores is the secondary growth of new zircon around an older core.

These issues are often identified during data analysis and can be identified when data is plotted on Wetherill and Tera-Wasserburg diagrams. Wetherill diagrams help identify issues within two or more isotopic systems (Wetherill, 1956). In the U-Pb system, Wetherill diagrams plot the ratios of the two U-Pb isotope systems: $^{206}\text{Pb}/^{238}\text{U}$ and $^{207}\text{Pb}/^{235}\text{U}$ (Spencer et al., 2016). If there are no detectable common Pb or inheritance issues, the data will plot on the concordia curve (Wetherill, 1956). Zircon grains which are plotted on this line are considered concordant which signifies there have been no apparent issues within the isotopic systems plotted. Concordant U-Pb ages are some of the most robust measurements of age in a geologic sample and are often considered as the gold standard of geochronology (Ludwig, 1998; Zi et al., 2022). Discordant zircon grains will plot away from this linear array. Discordant grains signify a disagreement of isotopic dates between two isotopic systems plotted (Wetherill, 1956). To help interpret data showing signs of Pb issues, the data is often plotted on Tera-Wasserburg diagrams.

Tera-Wasserburg diagrams are used to help understand the discrepancies between the measured U/Pb values and the radiogenic Pb values (Tera & Wasserburg, 1972). These diagrams usually plot the ratios of $^{207}\text{Pb}/^{206}\text{Pb}$ and $^{238}\text{U}/^{206}\text{Pb}$. If there is no evidence of inheritance, a best fit line can be plotted through the data points to determine an age based on the intercept with concordia (Ludwig, 1998). This line

serves as a graphical representation of the mixture of common Pb and radiogenic Pb defined by the data array. If there is no detectable variation in radiogenic Pb (i.e., the measurement precision cannot distinguish a different radiogenic Pb component), the location where the best fit line intercepts the concordia on a Tera-Wasserburg diagram can be interpreted as the radiogenic Pb component and represents the best age for the samples plotted (Ludwig, 1998).

Section I.E. Potential Sources of Craigs Hill Tephra

Two potential candidates as magmatic sources for the tephra layer approximately 5 million years ago would be either the Cascade Arc or Yellowstone-related eruptions. The ancestral and modern Cascade volcanic arcs formed after the initiation of Cascadia subduction approximately 55 Ma (Stern & Dumitru, 2019). This subduction zone is still active and is the source of the modern Cascade Arc volcanism.

The Heise volcanic field is a late Miocene to early Pliocene volcanic center with eruptions spanning 6.62 to 4.45 Ma (Bolte et al., 2015). There are several major eruptions which took part in the Heise volcanic field. The Blacktail Creek Tuff was formed from the first large eruption at the Heise volcanic center around 6.62 Ma (Watts et al., 2011). Other major eruptions occurred at 6.27 Ma, 5.57 Ma, 5.51 Ma. The final eruption at the Heise volcanic center occurred at 4.45 Ma and deposited the Kilgore Tuff (Bolte et al., 2015).

Using the $^{40}\text{Ar}/^{39}\text{Ar}$ derived age of 4.9 ± 0.1 Ma (Lamb, 1997) as a guide, it's clear the Cascade Arc and Yellowstone related eruptions were both active around this

period. Being armed with only a date, it is impossible to rule out either of these potential sources.

Chapter II: Methods

Section II.A. Extraction of Heavy Minerals

The tephra was collected from Craigs Hill by Nick Zentner and the sample location matches that of Lamb (1997). It is buff colored and consists of a mixture of clay to pebble sized grains. Some clots, perhaps weak concretions, are found within the sample and easily break apart when manipulated with hand or lightly squeezed. The grain size is dominantly clay-silt sized grains but there are larger grains present.

To filter out larger clumps of material, the sample was passed through series of sieves with the smallest being rated for $>149 \mu\text{m}$. The sample at the bottom sieve was extracted and placed into a container. The container was filled approximately halfway with hydrogen peroxide and placed in an ultrasonic bath for approximately one hour. The mixture was agitated with a glass stirring rod approximately every 10 minutes to prevent flocculation of clay grains within the mixture. After sonication, the sample was carefully decanted with distilled water to wash out clay grains and other light minerals. After drying, several vials of unconsolidated sediment were collected.

To extract zircon grains and phosphates from the unconsolidated sediment, a density-based separation technique was used. Two centrifuge tubes were filled with approximately 0.50 grams of the recovered sediment and acetylene tetrabromide, $\rho=2.96 \text{ g/cm}^3$. Tube 1 contained 0.50 grams of sediment and 10 ml of acetylene tetrabromide. Tube 2 contained 0.51 grams of sediment and 10 ml of acetylene

tetrabromide. The tubes were placed in the centrifuge for 2 minutes and then rotated within the centrifuge by 180° and then centrifuged again.

The centrifuge tubes were dipped slowly into liquid nitrogen approximately half of the length of the tube. The tubes were dipped in the liquid nitrogen until the bottom half of the tubes were completely frozen. The top half of the tubes were emptied into a waste container. The frozen half of the tubes were rinsed with acetone as a neutralizing agent. The combined sample was then washed again with acetone ten times and allowed to evaporate and dry. To extract additional phosphate and zircon, the density-based chemical separation process was repeated. The sample was transferred into a glass dish for handpicking of grains. The dish was filled with ethanol and several minerals were noted under the microscope including dark-greenish colored amphibole with prominent cleavage planes, apatite and other opaque minerals, and several other dark-colored mafic minerals. Zircon was not readily observed. Approximately 150 phosphate grains were handpicked and extracted with a pipette.

Zircon grains were extracted in two sessions. A total of 0.2669 grams of heavy minerals, $\rho > 2.96 \text{ g/cm}^3$, was transferred to a beaker for digestion in HF. The sample and a mixture of 5 ml of 2 M HF and 6 M HCl were added to a teflon beaker. The beaker was left on a hotplate overnight at 110 °C. The next day, an additional 5 ml of 2 M HF (Hydrofluoric Acid) and 6 M HCl were added to the beaker and allowed to dry overnight on a hotplate at 110 °C. The next step involved adding 4 ml of twice distilled HNO₃ at ~8 M and left on a hotplate overnight at 110 °C. This step was repeated the next day. Four ml of 6 M HCl was then added to the sample and allowed to dry. The following day, an additional 4 ml of 6 M HCl was added to the sample and left on a hotplate at 110 °C.

The sample was then extracted from the beaker and pipetted into a centrifuge tube. The tube was centrifuged for 3 minutes, rotated 180° and then centrifuged for an additional 2 minutes. The remaining HCl was carefully extracted with a pipette. Two ml of ultra-pure Milli-Q water was added to the centrifuge tube. After being centrifuged, the water was carefully extracted with a pipette. Ethanol was added to the centrifuge tube and the sample was carefully extracted with a pipette and placed in a cleaned petri dish for microscopic examination. About 10 zircon grains were identified and placed in the center of the dish. Tape was used to extract the grains from the petri dish. The tape with the zircon grains was then mounted on a glass slide and prepared for laser ablation.

To extract additional zircon, 0.5624 grams of heavy minerals, $\rho > 2.96 \text{ g/cm}^3$, were extracted and transferred to a beaker for digestion. To digest everything except zircon, HF and HNO₃ were used. Four ml of ~29 M HF and 0.5ml of ~15 M twice distilled HNO₃ were added to the beaker. The beaker was then placed on a hot plate at 110 °C for 3 days. After three days, the sample was transferred to a 15 ml centrifuge tube and excess HF was extracted and discarded. Eight ml of ultra-pure Milli-Q water was added to the centrifuge tube and the sample was centrifuged for 3 minutes. Excess fluids were extracted with a pipette and discarded. This was repeated three times. The remaining solid material was treated with 10 ml of ~8 M HCl and placed on a hotplate overnight at 110 °C.

The sample was centrifuged for 3 minutes, rotated 180° and centrifuged again for 2 minutes. The remaining HCl was extracted carefully with a pipette. Ten ml of ultra-pure Milli-Q water was added to the centrifuge tube. This was centrifuged for 3 minutes, rotated 180°, and then centrifuged again for 2 minutes. This was repeated 3 times. After

the remaining water was extracted, 10 ml of ethanol was added to the centrifuge tube. The contents of the tube were emptied into a petri dish for extraction of zircon grains via handpicking.

Approximately 50 zircon grains were identified with a microscope. The grains were notably small. Most of the grains were sub-rounded to rounded, approximately 25-50 μm in length. There were several elongate, euhedral grains which were significantly larger, <80 μm in length. The grains were centered in the middle of the petri dish and the ethanol was allowed to evaporate. The grains were then mounted in epoxy resin and polished to expose the zircons with 3000 grit sandpaper.

Section II.B. In Situ U-Th-Pb Isotope Analysis of Zircon

U-Th-Pb isotope analysis of zircon grains was conducted using a Jena *PlasmaQuant Elite* quadruple inductively coupled plasma-mass spectrometer (ICP-MS) coupled to a PhotonMachines *Excite* laser ablation instrument located at the University of Houston. Analyses were conducted in two sessions. The first session used a 25 μm diameter laser beam at 8 Hz repetition rate and for 30 seconds ablation time to analyze 4 zircon grains mounted on tape. Some grains which were large enough for multiple ablations were targeted several times. Calibration standards used were Plesovice Zircon and FC5Z Zircon (e.g., Slama et al., 2008; Shaulis et al., 2010). The following isotope values were measured: ^{202}Hg , ^{204}Hg , ^{204}Pb , ^{206}Pb , ^{207}Pb , ^{208}Pb , ^{232}Th , ^{232}U , ^{235}U , and ^{238}U . Due to a smaller grain size, the seconds session used a 20 μm diameter laser beam at 8 Hz repetition rate and for 30 seconds ablation time to analyze 43 zircon

grains mounted in epoxy resin. All other operation parameters are the same as the first session.

The laser ablation data was imported into Igor Pro for background subtraction and data window selections. Background-subtracted data were processed following methods outlined in Shaulis et al. (2010) and ages and concordia plots were calculated using Isoplot 3.7 software (Ludwig, 2000).

Section II.C. Neodymium Isotope Analysis

Approximately 150 grains of phosphate minerals were handpicked from the sample and placed in a beaker for Nd Isotope analysis. To digest the phosphate minerals, 5 ml of 6 M HCl was added to the beaker and placed on a hotplate overnight at 110 °C. After drying overnight, an additional 5 ml of 6.0 M HCl was added to the beaker and left on the hotplate overnight at 110 °C.

The digested sample was run through two sets of ion-exchange columns to isolate Rb, Sr, Sm and Nd. 200 µl of 2.5 M HCl was added to the sample and left overnight to ensure it was completely dissolved before column chemistry. The first set of columns uses AG 50Wx8 200-400 Mesh resin. The resin was cleaned by passing 10 ml of 6 M HCl through the resin twice. The resin was equilibrated and floated with 2.5 M HCl three times. The sample was then loaded in 200 µl of 2.5 M HCl and pipetted into the column. 0.5 ml of 2.5 M HCl was passed through the column two times. 10 ml of 2.5 M HCl was then passed through the column, followed by 8.5 ml of 2.5 M HCl. The rare earth elements (REE) were collected by passing 10.0 ml of 6.0 M HCl through the

column and into a clean beaker. This was done by passing 1.0 ml of 6.0 M HCl through the column, and then passing 9.0 ml of 6.0 M HCl through the column.

The second set of columns for Nd separation uses Ln-Spec resin. To prepare the sample for Nd separation column chemistry, 50 μ l of 1.0 M HCl was added to the sample and left overnight. The following day, 150 μ l of twice distilled H₂O was added to the sample. The resin was prepared and loaded into the column. The column was cleaned by passing one full column volume of 6 M HCl. Three runs of 1 ml twice distilled H₂O were then passed through the column. The column was then conditioned by passing 5 ml of 0.25 M HCl through the column in increments of 1 ml, 1 ml and then 3 ml.

The sample was loaded into the column with 200 μ l of 0.25 M HCl. 300 μ l of 0.25 M HCl was passed through the column in three increments of 100 μ l. 1.5 ml of 0.25 M HCl was passed through the column afterwards. To collect the Nd fraction, 3 ml of 0.25 M HCl was passed through the column and collected in a clean beaker. To prepare the Nd fraction for multi collector inductively coupled mass spectrometry (MC-ICP-MS), the Nd fraction was allowed to dry. 50 μ l of concentrated, twice distilled HNO₃ was added to the sample and then dried down. After drying completely, 1 ml of 2% HNO₃ was added to the sample for MC-ICP-MS. The Nu-Plasma II multi collector inductively coupled mass spectrometer at the University of Houston was used for analyzing the Nd fraction for this sample using methods outlined in Lapen et al. (2004; 2017).

Chapter III: Results

Section III.A. LA-ICP-MS of Zircon

Of the 47 zircon grains analyzed by LA-ICP-MS, the zircon ages range from approximately 4 Ma to over 2 Ga. Figure 3 shows a Wetherill concordia diagram for all zircon grains analyzed. There are several clusters of grains seen. Figure 4 is a higher resolution view of ages < 120 Ma; there are several notable clusters at approximately 90 Ma, 70-80 Ma, and 5 Ma. Many of the older grains plotted in Figure 3 and youngest grains in Figure 4 are discordant. LA-ICP-MS U-Pb dating of the zircon grains show a significant cluster of grains approximately 4 Ma. There are 12 grains in this approximately 4 Ma cluster. Several grains were large enough to be targeted multiple times with the laser. We collected data for 18 laser ablation target locations. A Tera-Wasserburg concordia diagram created from this cluster of grains shows an intercept age of 4.15 ± 0.10 Ma (Figure 5). A larger zircon grain was analyzed in three different locations and determined to be 6.5 ± 0.30 Ma (Figure 6). Figure 7 shows a weighted mean age of the three laser shots on the zircon grain. Figure 8 shows a Tera-Wasserburg concordia diagram for zircon grains approximately 70-80 Ma. No age intercept is calculated in this figure. Figure 9 is a Tera-Wasserburg concordia diagram for the grains of zircon approximately 90 Ma. The intercept in this figure shows an age of 90.3 ± 4.8 Ma. Figure 10 shows a weighted mean average of the grains approximately 90 Ma which shows a mean of 91.4 ± 2.4 Ma.

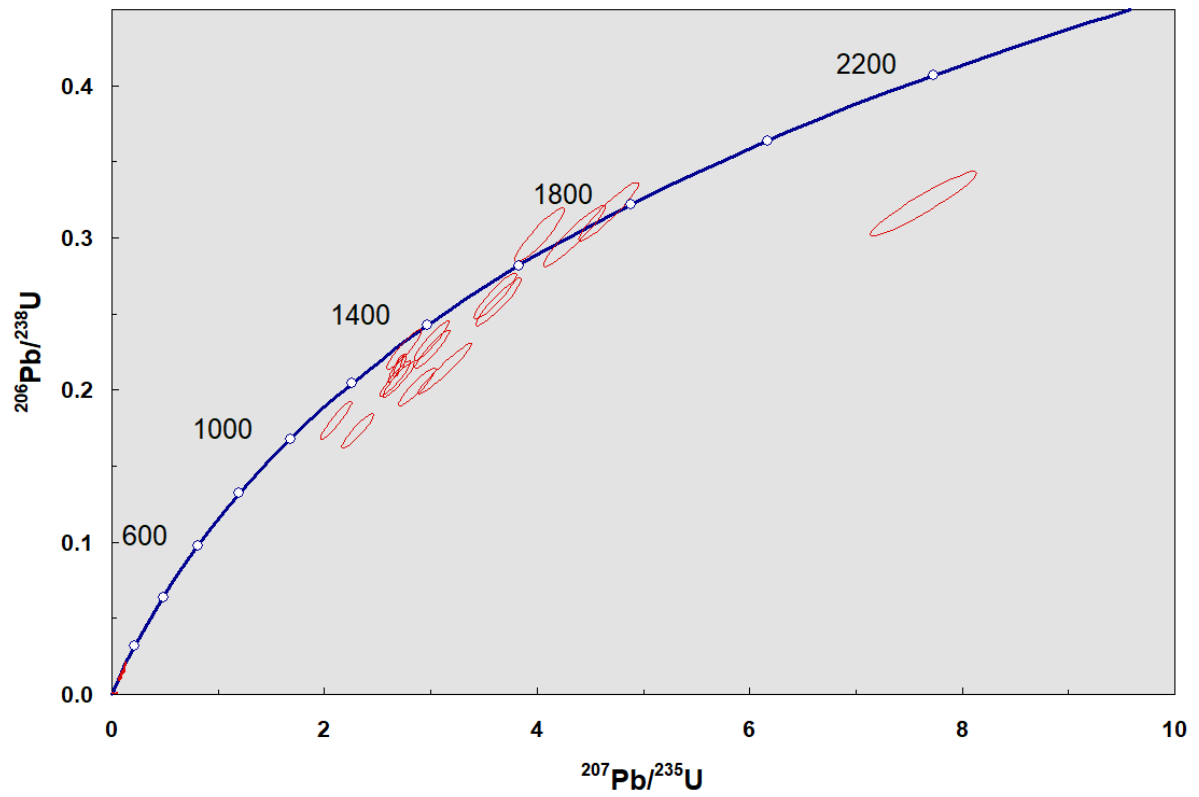


Figure 3: Wetherill concordia diagram for all zircon grains analyzed. Significant clusters are seen at under 110 Ma, 1400 Ma and 1800 Ma. Discordance is observed in grains plotted off the concordia curve.

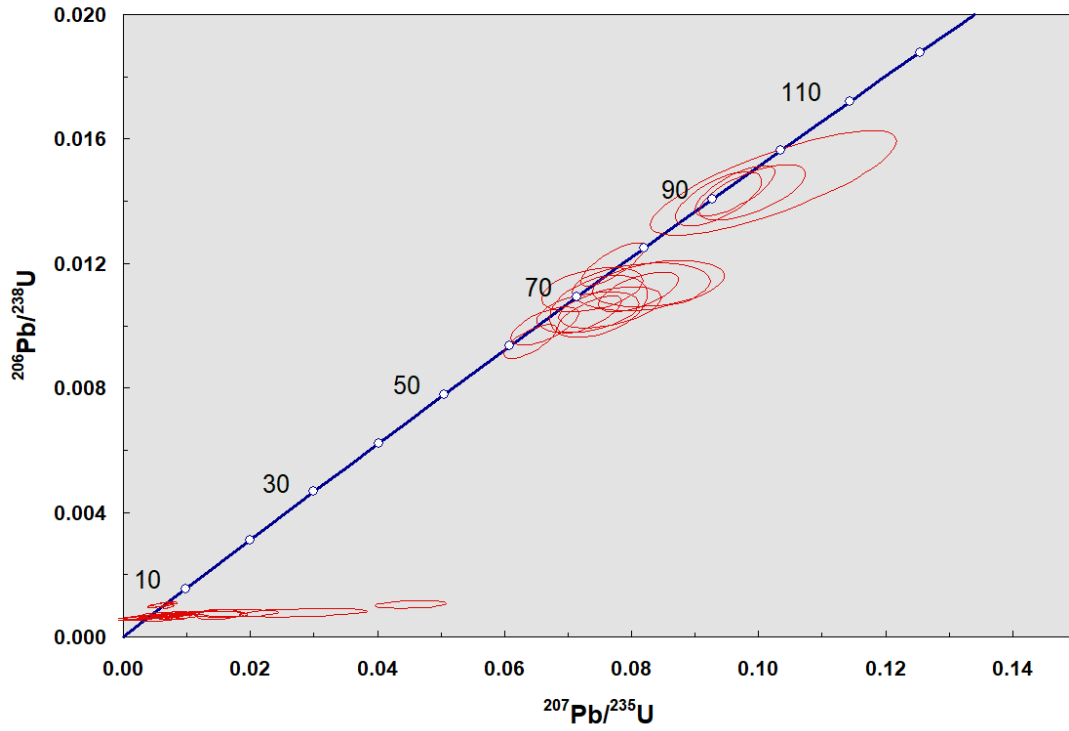


Figure 4: Wetherill concordia diagram for all zircon grains aged 110 Ma. Significant clusters are seen at approximately 5 Ma, 70 Ma, and 90 Ma. Discordance is observed in younger grains approximately 4 Ma.

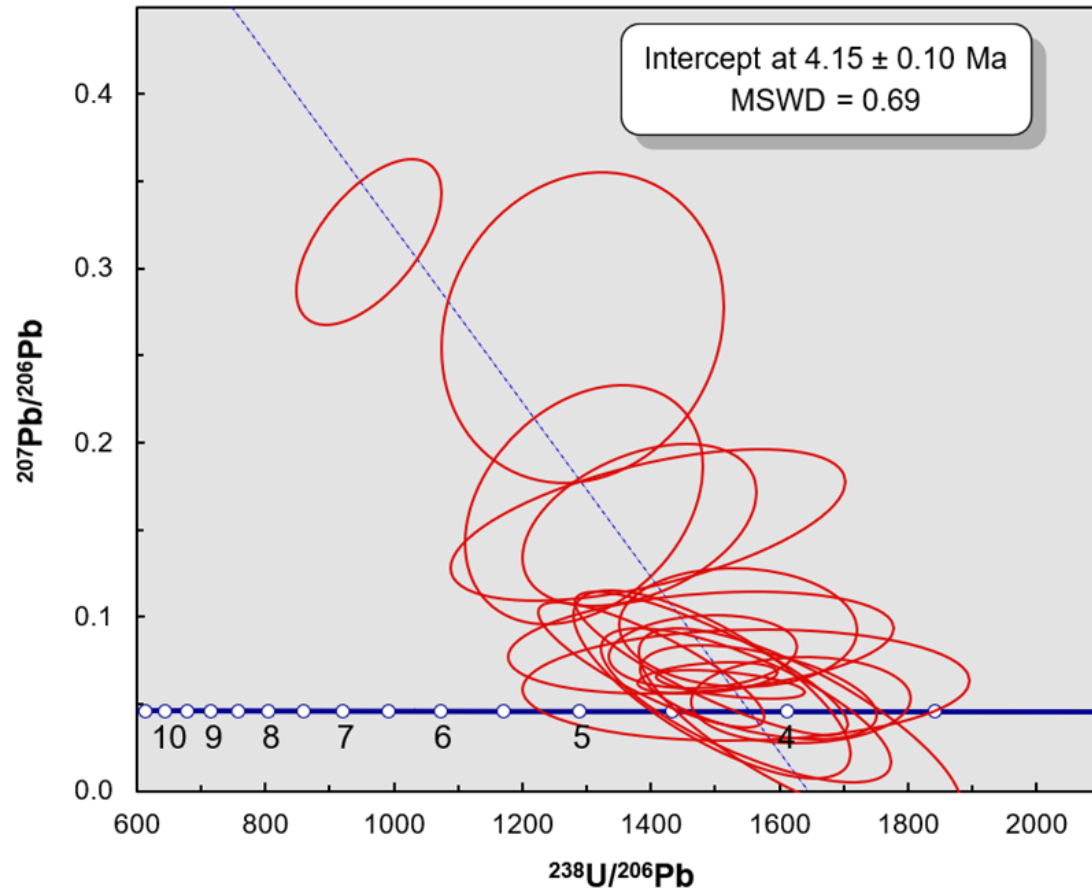


Figure 5: Terra-Wasserburg concordia diagram for all grains approximately 4 Ma. Best fit line intercepts concordia curve at 4.15 ± 0.10 Ma. This chart shows information for 18 laser ablation targets.

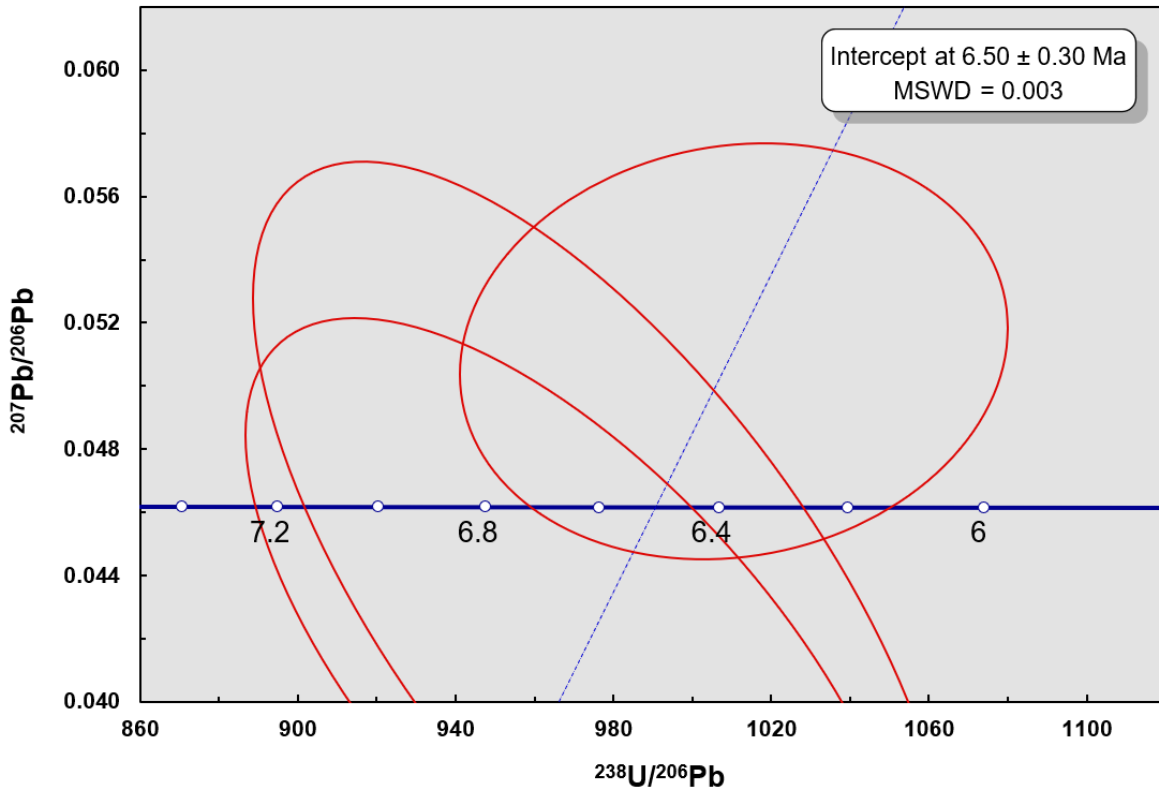


Figure 6: Tera-Wasserburg concordia diagram for a single 6.5 Ma zircon grain which was analyzed in three locations. Best fit line intercepts concordia curve at 6.50 ± 0.30 Ma.

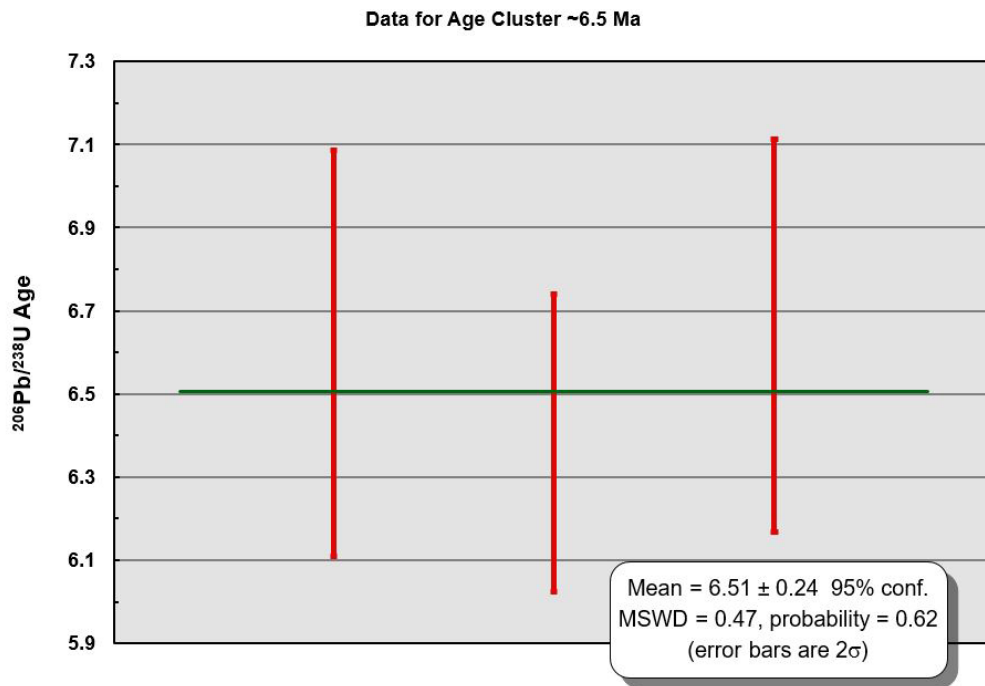


Figure 7: Weighted mean age plot for zircon grain approximately 6.5 Ma. Red bars represent $^{206}\text{Pb}/^{238}\text{U}$ apparent age range for laser ablation target locations. Each red bar represents one laser target.

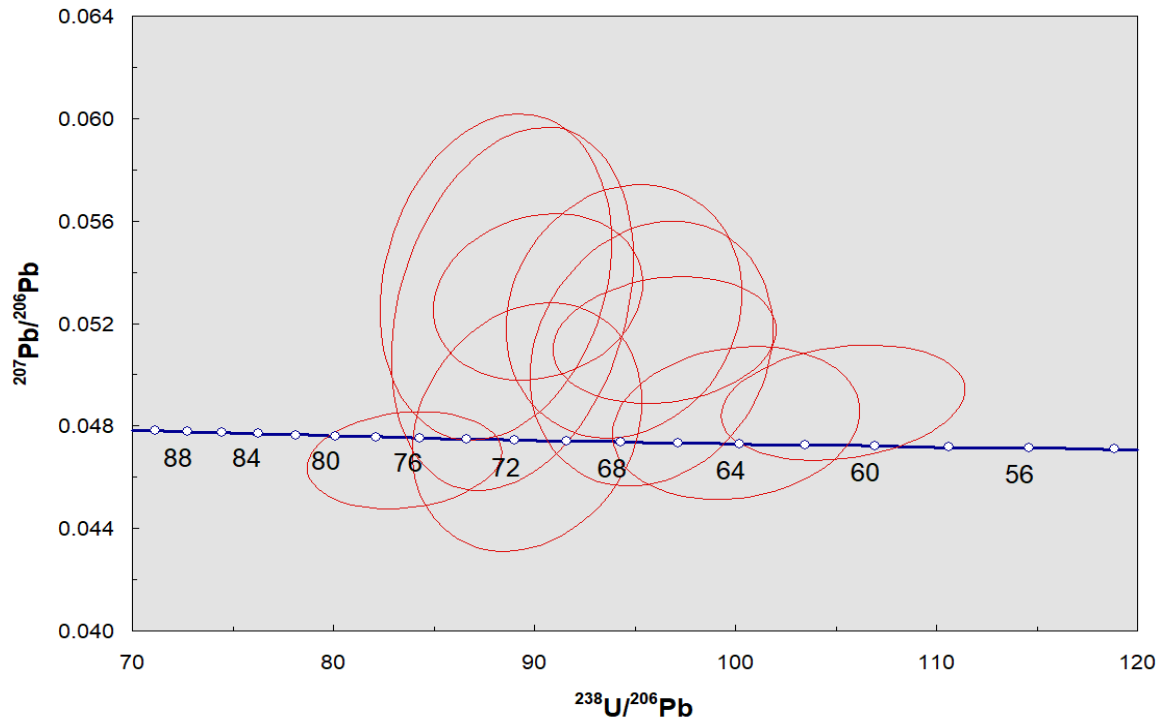


Figure 8: Tera-Wasserburg Concordia Diagram showing grains approximately 70-80 Ma. Due to the wide range of ages, no age intercept is calculated in this figure.

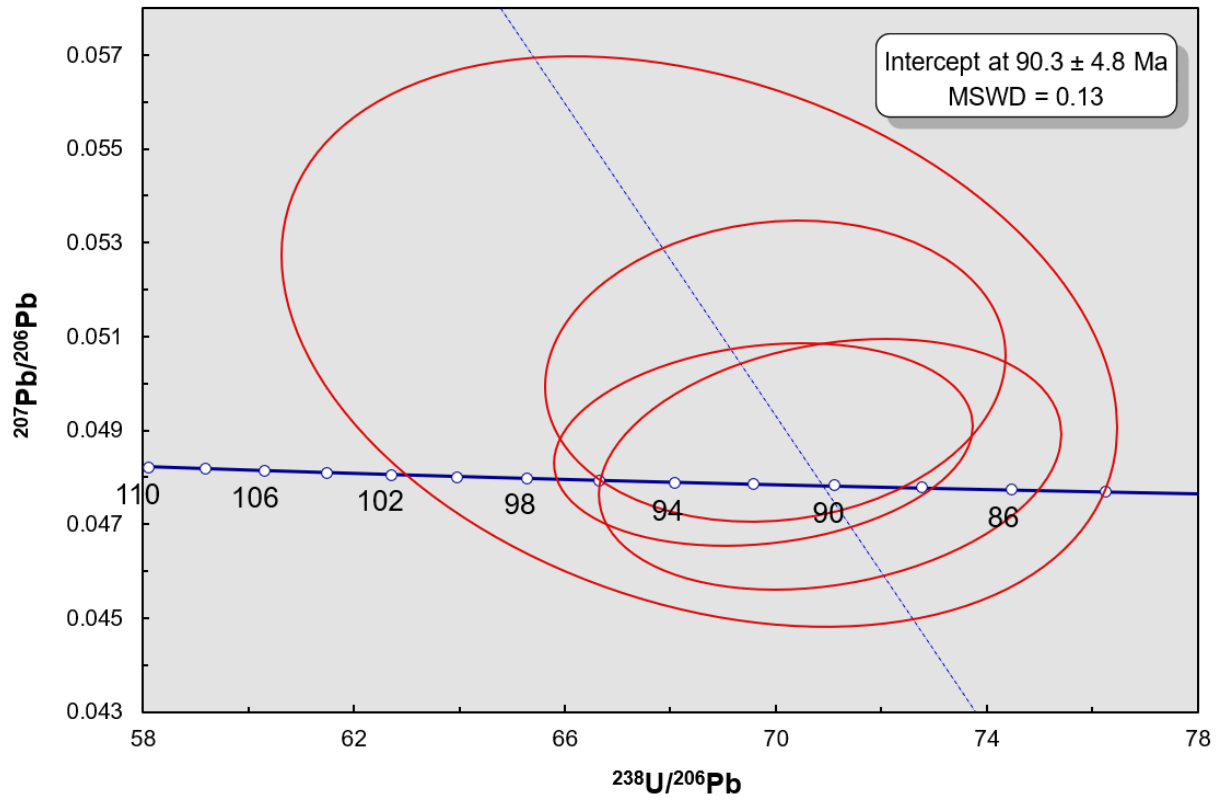


Figure 9: Tera-Wasserburg concordia diagram for 4 zircon grains approximately 90 Ma. Best fit line intercepts concordia curve at 90.3 ± 4.8 Ma.

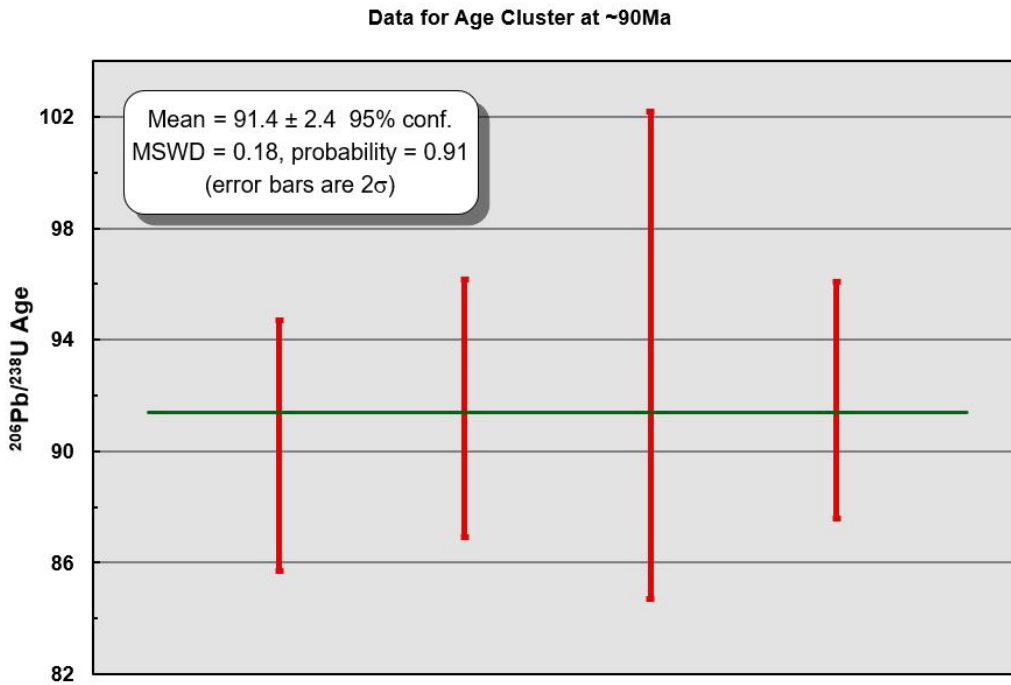


Figure 10: Weighted mean age plot for zircon grains approximately 90Ma. This data is collected from 3 individual zircon grains with one grain being targeted twice. Red bars represent $^{206}\text{Pb}/^{238}\text{U}$ apparent age range for laser ablation target locations. Each red bar represents one laser target.

Section III.B. MC-ICP-MS of Phosphate Minerals

Multi collector inductively coupled mass spectrometry was used to measure the $^{143}\text{Nd}/^{144}\text{Nd}$ ratio of 0.512988 which corresponds to a present-day ϵ_{Nd} of +6.83. Rock standards BIR-1A and BHVO-2 were used as standards. Pure Nd Jndi and AMES were solution standards prepared at University of Houston. Table 1 shows data collected from MC-ICP-MS for the Craigs Hill tephra. The ϵ_{Nd} value was calculated using the equation in Figure 11.

Table 1: MC-ICP-MS data for Craigs Hill Tephra. Solution standards are Pure Nd Jndi and AMES. Rock are standards BIR-1a and BHVO-2.

Sample ID	Sample Name	$^{143}\text{Nd}/^{144}\text{Nd}$	error (%)	$\epsilon^{143}\text{Nd}$
23-1	Indian Trail Phosphate	0.512988	0.002	6.83
22NH100	BIR-1a	0.513100	0.005	9.01
22NH101	BHVO-2	0.512987	0.005	6.81
	Jndi (UH) n=7	0.512115	0.0016	
	AMES (UH) n=4	0.511990	0.002	
	reference value			
	BIR-1a	0.513091	0.0014	
	BHVO-2	0.512979	0.0014	

$$\epsilon_{\text{Nd}} = \left[\frac{(^{143}\text{Nd}/^{144}\text{Nd})_{\text{sample}} - (^{143}\text{Nd}/^{144}\text{Nd})_{\text{CHUR}}}{(^{143}\text{Nd}/^{144}\text{Nd})_{\text{CHUR}}} \right] \times 10000$$

Figure 11: Equation used for calculating ϵ_{Nd} . 0.512638 used for $(^{143}\text{Nd}/^{144}\text{Nd})_{\text{CHUR}}$

Chapter IV: Discussion

Section IV.A. Questions Surrounding the Age of the Tephra Layer

The tephra unit currently designated as being part of the Ellensburg Formation (Figure 2) has been previously dated to 4.9 ± 0.1 Ma using $^{40}\text{Ar}/^{39}\text{Ar}$ isotopes in hornblende grains (Lamb, 1997; Figure 12). A new date of 4.15 ± 0.10 Ma for this tephra unit was calculated using U-Pb dating of zircon grains. The U-Pb age is significantly younger than the $^{40}\text{Ar}/^{39}\text{Ar}$ derived date presented in Lamb (1997). The approximately 800,000-year difference in ages could be related to excess argon, which can be an issue for young, K-poor materials such as the analyzed hornblende. Another potential cause for the age discrepancy could be older, detrital hornblende grains being included in the $^{40}\text{Ar}/^{39}\text{Ar}$ analysis.

Figure 12 is an updated stratigraphic column of Craigs Hill. The tephra layer marked with a yellow triangle labeled “4.9” in Figure 2 has been updated to a red triangle labeled “4.15”. Even though the age of the Ellensburg – Thorp contact is likely diachronous, it could be as old as ~ 4.7 Ma (Smith, 1988). It was decided to include this date in the stratigraphic column because this date is one of the only dates published in peer-reviewed literature. The date of ~ 4.7 Ma for this contact fits well with our new date for the tephra layer of 4.15 Ma. With the new 4.15 Ma date, a vertical succession of increasingly older dates from top to bottom is seen (Figure 12).

Section IV.A.i. Determining a Maximum Age of Deposition

When determining the maximum depositional age of a sample, the youngest single grain or youngest cluster of grains is commonly used to determine the maximum depositional age (Dickinson & Gehrels, 2009; Sharman & Malkowksi, 2020; Zi et al., 2023). The youngest single grain age is a simple but less precise method to determine a maximum depositional age (Dickinson & Gehrels, 2009; Sharman & Malkowksi, 2020). The most pressing issue with using the youngest single grain is the use of one data point which may be spurious or could have other uncertainties that could impact the measurements (Dickinson & Gehrels, 2009). Dickinson & Gehrels, (2009) defined the youngest cluster of grains as requiring more than three grains whose ages are indistinguishable within analytical uncertainty. Thus, the youngest cluster of grains that define an apparent two-component mixing line between common and radiogenic Pb was used to calculate the age of the unit. Using a single data point to define an age is impractical because there is no way of determining levels of contamination, crystal defects or other factors which could affect radiogenic dating.

If an apparent two-component mixture of radiogenic Pb and common Pb is identified within a series of analyses, it is necessary to correct for this (e.g., Figure 5). Common Pb corrections can be done by plotting co-genetic grains with variable radiogenic and common Pb ratios on concordia or isochron plots (Ludwig, 1998; Chew et al., 2014). In Wetherill concordia diagrams of our zircon grains (Figures 3 and 4), a large degree of discordance is seen in the youngest cluster of grains. The youngest cluster of grains spreads out to the right of the concordia which is evidence of Pb

mixing. To correct for the mixture of radiogenic Pb and common Pb, the data was plotted on a Tera-Wasserburg diagram (Figure 5) using Isoplot 3.7 (Ludwig, 2000).

Several discordant grains (i.e., grains that do not overlap with concordia within 2 standard deviations of the mean) were identified, the majority of grains plot on or near the concordia curve. There is no evidence in the data to indicate any statistically distinguishable radiogenic Pb isotopic compositions that would indicate younger ages. The best fit line plotted through the data ellipses intercepts with concordia curve to show a true radiogenic Pb isotopic composition and corresponding best age of 4.15 ± 0.10 Ma.

Section IV.A.ii. Could Excess Argon Explain the Different Ages?

While $^{40}\text{Ar}/^{39}\text{Ar}$ is a well-known and widely used tool in geochronological studies, there can be excess Ar issues with this dating technique applied to young, K-poor materials. In the appendices presented in Lamb, (1997), the lab reports followed an $^{40}\text{Ar}/^{39}\text{Ar}$ procedure which defined an argon release plateau as 3 or more contiguous heating steps in which at least 50% of the ^{39}Ar is released. It is noted in the reports during initial heating steps, distinct argon reservoirs were released which could have been the result of excess argon within fluid or melt inclusions within the hornblende grains (Lamb, 1997).

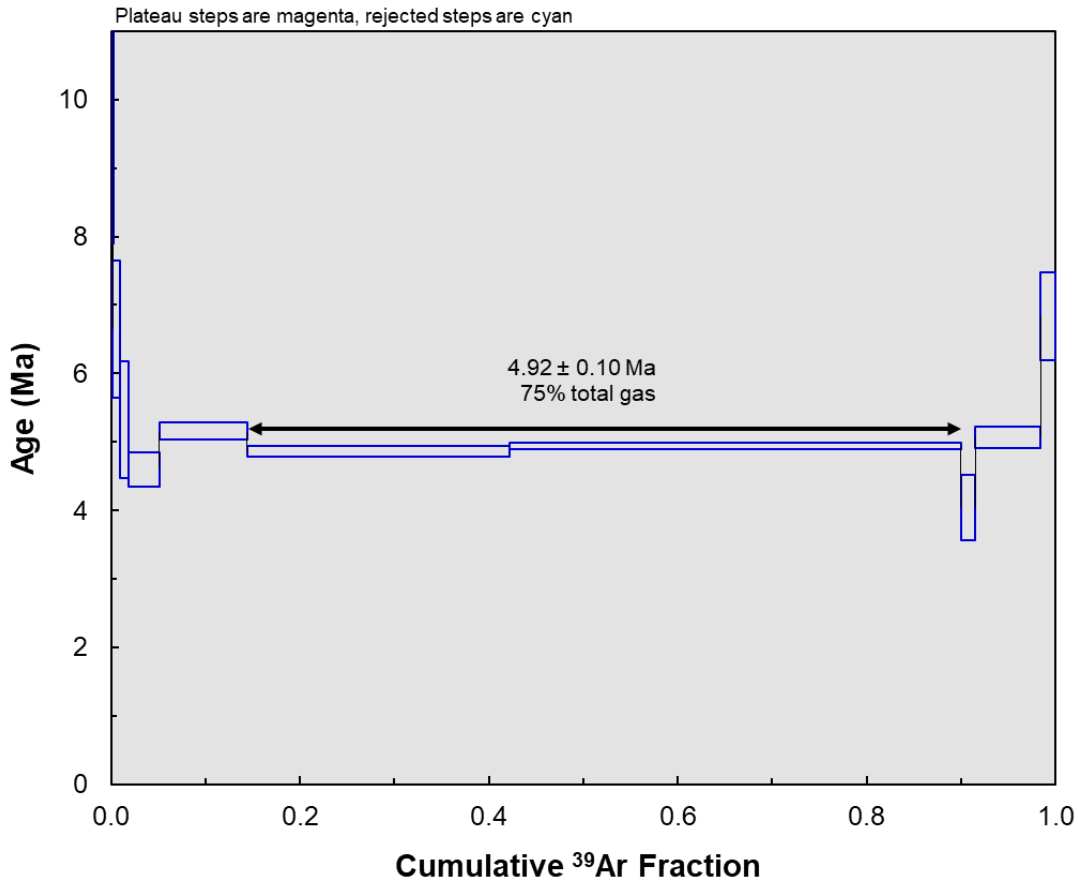


Figure 13: Argon release spectra data from Lamb, (1997). This plot shows the saddle-shaped spectra typical of excess argon.

Updated guidelines for interpreting $^{40}\text{Ar}/^{39}\text{Ar}$ data determined a plateau must consist of 5 or more consecutive steps in which at least 50% of the ^{39}Ar is released and should be between 15-40 heating increments (Schaen et al., 2021). It is also noted caution should be used when reporting dates calculated with a loosely defined plateau involving less than 5 consecutive steps and suggested other dating techniques be performed to confirm the age of a sample (Schaen et al., 2021).

Figure 12 shows the argon release spectra used to date the Indian Trail hornblende grains located in the tephra unit of Craigs Hill. This saddle-shaped spectrum is expected to occur when excess argon is playing a role in dating a mineral (Kelley,

2002; Schaen et al., 2021). As explained in Schaen et al. (2021), excess argon and loose definitions of an argon release plateau should be used with caution when reporting ages because of possibilities of reporting an inaccurate age. Erroneously older ages reported using $^{40}\text{Ar}/^{39}\text{Ar}$ dating techniques are not uncommon (Krummenacher, 1970).

Section IV.A.iii. Detrital Hornblende Possibly Included in Analysis

As seen in the results section of this paper, there is a significant amount of detrital zircon in the Craigs Hill tephra. If there is such a significant amount of detrital zircon, it would not be unreasonable to assume other detrital material must be present in the tephra as well.

In this study, we had an advantage of being able to analyze zircon grains individually, whereas the $^{40}\text{Ar}/^{39}\text{Ar}$ dating technique used a multi-grain aliquot of 62 mg of hornblende analyzed together to generate the argon release spectra (Lamb, 1997). Overall, $^{40}\text{Ar}/^{39}\text{Ar}$ dating relies on determining the amount of ^{40}Ar which has accumulated within a mineral over time due to ^{40}K decay (Kelley, 2002; Schaen et al., 2021). This means older hornblende grains would have accumulated more argon than younger hornblende grains. If older detrital hornblende grains were analyzed simultaneously with younger grains, the heating process would release more ^{39}Ar and yielded an older apparent age which would represent a mixture, not the true age of the unit.

Section IV.B. Detrital Zircons Within the Tephra

Within the tephra layer, there are detrital zircons which suggest this ash layer was not deposited as a single ash-fall event but was likely somewhat reworked. This could be due to volcanic eruptions resulting in turbulent flows that incorporate other material into the ash column. As evidenced from the ages of the grains, zircon grains from many geologic formations are present within this tephra layer. The presence of detrital zircons of many different ages is expected due to the level of volcanic activity and tectonic deformation this region has experienced. In the Wetherill plot of all zircon grains studied (Figure 5), many of the older grains are discordant and plot off the concordia curve. This can be interpreted as lead loss due to metamorphism or other significant events in the mineral's history. Metamorphic modifications to the zircon grains appear to be quite common in the older grains due to the geologic history of the region.

Section IV.C. Swakane Gneiss Zircon Signatures Found in Craigs Hill?

A recent study of zircon samples extracted from the Swakane Gneiss show the zircon ages vary significantly (Sauer et al., 2020). This study found the dates were dominantly Mesozoic or Proterozoic and contained distinct core, mantle, and rim zones. The zircon samples all had multiple Mesozoic peaks at 160-140 Ma, 130-110 Ma, 100-70 Ma, and some showed minor peaks at 250-200 Ma. Proterozoic dates of the zircon samples ranged from 1800-1600 Ma and 1440-1360 Ma (Sauer et al., 2020). Using the detrital zircon pattern of the Swakane Gneiss sample it was concluded the Swakane

Gneiss protolith was derived from accretionary wedge or forearc units (Sauer et al., 2020).

Interestingly, many of the Craigs Hill zircon grains also fall into these age ranges. We had a total of 71 laser ablation targets and 20 of them dated to the Proterozoic. Of those 20 Proterozoic laser targets, 8 of them fall in the 1800-1600 Ma or 1440-1360 Ma groups. We had 8 targets which yielded Late Cretaceous (100-70 Ma) ages. We did not use cathodoluminescence to image the grains, so it is not known if we were targeting inherited cores, but the ages alone seem to suggest Craigs Hill has incorporated some similar detrital zircon ages to many of the Swakane Gneiss samples. Whether the zircons were directly sourced from the 'nearby' (~30-40 km) gneiss outcrops or some tertiary sedimentary units underlying the Columbia River Basalt Group (e.g., Roslyn Formation) is unclear and would require further study.

Section IV.D. Possible Source of ~90Ma Zircon Grains

The Mt. Stuart batholith is a Cretaceous-aged intrusion in the Northern Cascades. It is a calc-alkaline pluton composed a wide range of rocks with the dominant rock type being quartz diorite (Erikson, 1977). The Mt. Stuart batholith was emplaced into the Jurassic-aged Chiwaukum Schist and the Jurassic-aged Ingalls ophiolite sequence (Matzel et al., 2006). U-Pb geochronologic work on zircon grains determined the Mt. Stuart batholith is approximately 96 - 91 Ma (Matzel et al., 2006). Geologic maps of the Mt. Stuart batholith complex show ages of associated units range from 96 - 90 Ma (Miller et al., 2007). This batholith is approximately 60 km north of Craigs Hill in Ellensburg, WA. The simplest method to explain the transportation of detrital zircons

from the batholith to Craigs Hill would be transportation and deposition via water. The Yakima River and the system of creeks and streams which flow into it are responsible for draining portions of the Mt. Stuart batholith region. Near the Mt. Stuart complex, these rivers and streams generally flow southward towards the Kittitas Valley.

The meandering morphology of the Yakima River suggests the river formed on flat land which predates the local uplift of the region and deposition of the Columbia River Basalt Group. Several tributaries to the Yakima River flow from the Mt. Stuart region into the Yakima River. The current proximity of the Yakima River to the Ellensburg, WA area makes it a strong candidate for a depositional system capable of transporting detrital zircons ultimately shed from the Mt. Stuart batholith to the Kittitas Valley. The Yakima River is responsible for the deposition of the Thorp Gravel within the Kittitas Valley approximately 3.7 million years ago (Smith, 1988).

The Yakima fold and thrust belt in central Washington was developed within the Columbia River Basalt Group, the Ellensburg Formation and younger sedimentary units (Bender et al., 2016). The development of the Yakima folds is hypothesized to have occurred between 10.5 and ~2.9 Ma (Bender et al., 2016). South of Ellensburg, WA, and the study site of Craigs Hill, the Yakima River cuts a nearly 600m deep canyon across several of the Yakima Folds (Bender et al., 2016). The canyon serves as more evidence which proves the Yakima River predates the uplift and folding of the region and it could be responsible for bringing detrital material into the Ellensburg region and depositing it in Craigs Hill. The Yakima River could also be responsible for the erosion of the Upper Ellensburg Formation in Craigs Hill. The local disconformity between the Thorp Gravel (~3.7 Ma) and the preserved top of the Upper Ellensburg Formation (~4.7

Ma) shows a lengthy period non-deposition and erosion occurred (Smith, 1988; Smith et al., 1989). As seen in Figure 2, there appears to be an incised channel which cut into older portions of the Upper Ellensburg formation. Deposition of the Thorp gravel begins above this unconformity.

Section IV.E. Phosphate Nd Isotopic Composition

There were two primary suspect source regions of this tephra: Cascade Arc magmatism or eruptions linked to the Yellowstone Hotspot track. A $^{143}\text{Nd}/^{144}\text{Nd}$ value of 0.512988 and corresponding ϵ_{Nd} value of +6.83 was determined by the ~150 phosphate grains digested and analyzed by MC-ICP-MS. To establish a correlation between a depleted mantle source or enriched mantle source, the values were compared to Nd compositions found in samples taken from the Quaternary Mount Adams volcanic field and samples taken from Yellowstone.

Mount Adams is in southern Washington, approximately 50km east of Mount St. Helens. It is the second most voluminous volcano in the Cascades (Sherrod and Smith, 1990). A previous study of isotopic values of 30 Quaternary lava flows from the Mount Adams stratovolcano and its associated volcanic field found ϵ_{Nd} values ranged from +5.35 to +7.24 with most values being near ~+6 (Jicha et al., 2009). The $^{143}\text{Nd}/^{144}\text{Nd}$ and ϵ_{Nd} values of the Mount Adams volcanic field are remarkably close to the values determined by MC-ICP-MS of Craigs Hill phosphate grains presented in this paper.

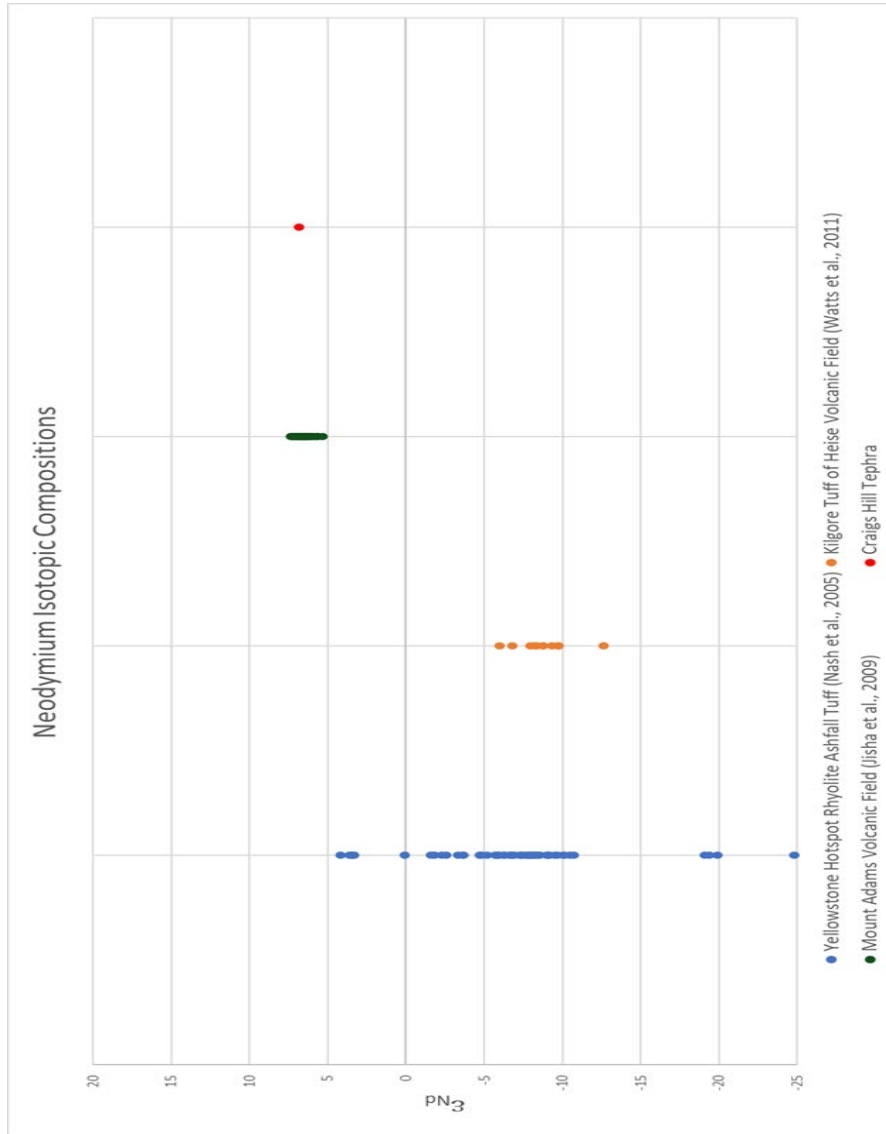


Figure 14: Graph comparing ϵ_{Nd} values of Craigs Hill tephra to three other samples. Yellowstone Hotspot Rhyolite Ashfall Tuff (Nash et al., 2005), Kilgore Tuff of Heise Volcanic Field (Watts et al., 2011), Mount Adams Volcanic Field (Jisha et al., 2009) and Craigs Hill.

To compare Craigs Hill tephra ϵ_{Nd} values to Yellowstone related eruptions, we compared our results to a study of over 50 Yellowstone Hot Spot rhyolite ash-fall tuffs with dates ranging from 15.9 to 0.4 Ma (Nash et al., 2006) and samples of the Kilgore Tuff of the Heise volcanic field (Watts et al., 2011). The rhyolite ash-fall tuff ϵ_{Nd} values ranged from -24.8 to 4.2. The highest ϵ_{Nd} value of 4.2 was found in ~16 Ma silicic ash ash-fall tuffs (Nash et al., 2006). Positive ϵ_{Nd} values were found to correlate mostly with the Columbia River flood basalts and negative ϵ_{Nd} values were found to correlate with

Yellowstone Hotspot rhyolites (Nash et al., 2006). The ϵ_{Nd} values of the Kilgore tuff samples ranged from -6.01 to -12.64 (Watts et al., 2011).

Our phosphate minerals primarily consisted of apatite. Apatite incorporates a wide variety of elements into its lattice and is increasingly being studied as a geological tracer (O'Sullivan et al., 2020). Although we did not measure whole rock Nd values, it is viable to compare apatite Nd values to whole rock Nd values if the materials are sufficiently young such that there is no measurable radiogenic ingrowth of ^{143}Nd . It has been shown that apatite has a rare earth element composition that is closely related to its source rock (O'Sullivan et al., 2020). It's also been shown the source rock composition can be determined from apatite rare earth element analysis (O'Sullivan et al., 2020).

Using these reference materials, it was determined the Craigs Hill tephra layer phosphate Nd ratios closely resembled material from the Mount Adams volcanic field tephra sources likely originated from a shallow, depleted mantle source. This points to Cascade Arc magmatism as the primary source for this tephra layer.

Section IV.F. Implications for the timing of Cervidae in North America

The cervid fossil found within the paleosol layer directly under the Craigs Hill tephra was tentatively assigned to *Bretzia pseudalces* (Emery-Wetherell & Schilter, 2020). The assignment of *Bretzia* was due to the proximity of the Ringold Formation and fossils of *Bretzia* found within that formation. The Ringold Formation was deposited between 8 - 2 Ma (Reidel & Tolan, 2013). It is a sedimentary layer which was deposited

as the course of the Columbia River was obstructed by the deposition of the Columbia River Basalt group and deposited as the river eroded its way through the basalt deposits (Reidel & Tolan, 2013). The Ringold Formation is capped by the Pleistocene Missoula Flood deposits which occurred between ~2 Ma and 13,000 years ago (Bretz et al., 1956).

One of the earliest known occurrences of *Bretzia pseudalces* is within the Ringold Formation in Washington and is dated to ~5.0 - 4.8 Ma (Gustafson, 2015). This occurrence forms the upper constraint on the arrival of *Bretzia pseudalces* (Gustafson, 2015). The lower constraint of *Bretzia* is the Pleistocene-Holocene (Gunnel & Foral, 1994). These constraints impart a timeframe of ~5 Ma to ~10,000 years ago for *Bretzia*.

When taking the newly determined age U-Pb age of 4.15 ± 0.10 Ma into account, fossils of *Bretzia* are expected to be found within the deposits of Craigs Hill. The age of 4.15 ± 0.10 Ma falls in the relatively early existence of *Bretzia*, but by this time, *Bretzia* had already been an established species within the Ellensburg region.

Chapter V: Conclusion

The Craigs Hill tephra layer is a Pliocene-aged deposit with a newly assigned U-Pb age of 4.15 ± 0.10 Ma. This new age places this tephra unit within the potential age range of the Thorp Gravel (4.7 to 3.7 Ma) and was deposited directly above the Upper Ellensburg formation (~4.7 Ma). This age also fits well in line with existing studies on the other stratigraphic layers of the region.

Using the new U-Pb age of this tephra, it is determined that this tephra layer does not form one of the earliest constraints for the timing of Cervidae in North America. The earliest fossil of *Bretzia* was discovered in the Ringold formation (~5.0 Ma). If the ~5.0 Ma date of the Ringold formation is correct, then at 4.15 ± 0.10 Ma, *Bretzia* had already been an established species in North America for approximately 800,000 years.

Isotopic analysis of ~150 grains of phosphate minerals resulted in $^{143}\text{Nd}/^{144}\text{Nd}$ ratio of 0.512988 and ϵ_{Nd} of +6.83. This likely indicates a shallow, depleted mantle source. When compared other geologic samples of other potential source regions, these values are closely related to Cascade Arc magmatism. The source of the Craigs Hill tephra deposit is likely a volcanic event related to arc magmatism from the Cascade Range.

Appendices

Table 2: Argon release data from Lamb, (1997)

Indian Trail Ash Ar-Ar data										
62.63 mg hornblende										
J = 0.0007510										
	Temp	40Ar/39Ar	37Ar/39Ar	36Ar/39Ar	Ar _k Mol	K/Ca	%Ar40	%Ar39	Age	± 2 s.d.
					*10 ⁻¹⁶		Rad	Released	(Ma)	(Ma)
7208-01A	750	251.9	5.477	0.6968	0.128	0.093	18.4	0.076	62	31
7208-01B	850	42.33	9.426	0.0428	0.084	0.054	71.8	0.121	41	16
720B-01C	950	43.34	12.84	0.0931	0.098	0.040	38.8	0.184	22.9	15
7208-010	1050	6.458	9.083	0.0077	1.20	0.056	75.6	0.893	6.65	1
7208-01E	1080	4.35	8.957	0.0038	1.61	0.057	89.9	1.85	5.33	0.85
7208-01F	1110	4.887	8.943	0.0074	5.50	0.057	69.1	5.11	4.6	0.25
7208-01G	1130	4.653	8.945	0.0052	15.7	0.057	81.5	14.4	5.16	0.12
720B-01H	1150	4.691	8.474	0.006	47.0	0.060	76.1	42.2	4.86	0.08
7208-011	1180	4.15	8.369	0.0039	80.6	0.061	87.5	90	4.94	0.05
7208-01J	1220	4.548	9.757	0.0079	2.63	0.052	65.1	91.5	4.04	0.48
7208-01K	1300	4.592	9.507	0.0054	11.6	0.054	81	98.4	5.07	0.16
7208-01L	1650	12.64	10.05	0.0284	2.71	0.051	39.7	100	6.84	0.64
				n = 12	169	0.059			5.04	0.15 Total gas age

Table 3: Zircon LA-ICP-MS isotope data

Data	$^{207}\text{Pb}/^{206}\text{Pb}$		$^{207}\text{Pb}/^{235}\text{U}$		$^{206}\text{Pb}/^{238}\text{U}$		$^{208}\text{Pb}/^{232}\text{Th}$		
	Bias Corr.	2%SD	Bias Corr.	2%SD	Bias Corr.	2%SD	rho	Bias Corr.	2%SD
Zircon 1	0.0472	4.5078	0.0937	5.8980	0.0141	5.0329	0.6703	0.0048	6.9606
Zircon 2	0.0504	5.2073	0.0990	6.8941	0.0143	5.0879	0.6600	0.0049	5.9321
Zircon 3-1	0.0470	22.2355	0.0061	31.4079	0.0010	7.4029	0.8000	0.0005	21.0182
Zircon 3-2	0.0494	10.5340	0.0070	11.3724	0.0010	5.6118	0.3906	0.0003	12.3014
Zircon 3-3	0.0499	38.0080	0.0058	27.8799	0.0010	7.1132	0.8000	0.0003	24.8843
Zircon 4-1	0.1074	1.6792	4.6718	4.8926	0.3172	4.9306	0.9416	0.0966	4.7735
Zircon 4-2	0.1039	1.8098	4.3478	5.4435	0.3013	5.4610	0.9449	0.0931	4.9767
Zircon 5	0.0518	8.3218	0.0731	8.9555	0.0104	5.1491	0.4062	0.0032	11.2346
Zircon 6-1	0.0464	3.3188	0.0770	5.3198	0.0120	4.7376	0.7882	0.0036	7.5948
Zircon 6-2	0.0892	2.9032	0.6773	9.2373	0.0525	8.2194	0.9513	0.0233	9.2158
Zircon 6-3	0.0987	1.7976	1.2848	5.4036	0.0924	5.3829	0.9445	0.0374	5.1353
Zircon 7-1	0.0526	58.8609	0.0071	49.4799	0.0007	10.2872	0.8944	0.0002	38.1409
Zircon 7-2	0.0643	61.7510	0.0044	82.3212	0.0006	11.9030	0.8000	0.0003	38.4435
Zircon 7-3	0.0773	55.5418	0.0057	81.1349	0.0007	11.7945	0.8000	0.0001	100.0798
Zircon 7-4	0.0576	74.3631	0.0030	141.9928	0.0006	12.5878	0.8000	0.0003	52.9288
Zircon 7-5	0.8992	166.6685	0.0025	150.0543	0.0008	10.7158	0.8000	0.0002	48.3137
Zircon 8-1	0.1045	1.7171	3.1346	6.6195	0.2141	6.4250	0.9658	0.0616	7.2430
Zircon 8-2	0.0950	2.7421	1.4392	9.0083	0.1054	8.3729	0.9528	0.0463	9.5765
Zircon 9-1	0.0939	1.6813	2.6992	4.4280	0.2070	4.5932	0.9312	0.0744	4.6269
Zircon 9-2	0.0956	1.9401	4.0245	4.6916	0.3018	4.8166	0.9171	0.0840	4.9977
Zircon 10-1	0.0483	9.7621	0.1024	15.4883	0.0146	9.4299	0.7994	0.0038	7.5491
Zircon 10-2	0.0486	8.2673	0.0738	8.8453	0.0112	5.2125	0.4019	0.0036	6.5537
Zircon 11	0.0932	1.5982	3.0068	4.4586	0.2323	4.5692	0.9376	0.0719	4.2739
Zircon 12	0.0873	1.8870	2.7484	4.8120	0.2269	4.7492	0.9222	0.0649	4.4856
Zircon 13	0.0865	2.0075	2.1089	5.7406	0.1802	5.6671	0.9381	0.0617	4.4751
Zircon 14	0.0592	28.9239	0.0095	28.9951	0.0011	8.1074	0.1486	0.0002	60.1329
Zircon 15-1	0.0522	7.7024	0.0766	8.6034	0.0106	5.0745	0.4632	0.0035	6.0819
Zircon 15-2	0.0545	11.0368	0.0815	10.8903	0.0112	5.5385	0.2277	0.0037	9.1951
Zircon 16	0.2077	27.3655	0.0283	28.9951	0.0008	13.8698	0.3534	0.0008	20.3952
Zircon 17-1	0.0527	4.9949	0.0811	6.2966	0.0111	4.7157	0.6220	0.0041	7.8695
Zircon 17-2	0.0520	3.9317	0.0734	5.6221	0.0104	4.7000	0.7236	0.0033	5.1260
Zircon 18-1	0.1111	35.6167	0.0159	32.8073	0.0009	11.5339	0.0782	0.0006	22.5786
Zircon 18-2	0.1229	24.6148	0.0192	23.9009	0.0012	9.3401	0.1178	0.0008	20.2102
Zircon 19	0.0471	4.3262	0.0511	5.9150	0.0078	4.8322	0.6931	0.0022	8.1845
Zircon 20	0.0607	5.6645	0.1406	11.2092	0.0157	8.1225	0.8761	0.0155	15.3090
Zircon 21	0.0481	3.6266	0.0962	5.3467	0.0143	4.6528	0.7453	0.0043	5.4616
Zircon 22	0.0649	38.3344	0.0050	43.8226	0.0006	9.5705	0.6467	0.0002	16.0434
Zircon 22-2	0.0872	41.3867	0.0044	38.9850	0.0006	8.5622	0.1793	0.0002	11.9463
Zircon 23	0.1015	1.7616	3.6363	4.7408	0.2579	4.9733	0.9353	0.0794	4.3460
Zircon 24-1	0.1102	18.1985	0.0465	13.5972	0.0036	6.7998	0.5411	0.0019	14.1228
Zircon 24-2	0.0534	13.1564	0.0267	13.0161	0.0040	5.5793	0.1890	0.0012	10.4339
Zircon 25	0.0882	25.0122	0.0075	21.8053	0.0007	8.0768	0.2410	0.0002	10.6333

Table 3 Continued: Zircon LA-ICP-MS isotope data

Data	$^{207}\text{Pb}/^{206}\text{Pb}$		$^{207}\text{Pb}/^{235}\text{U}$		$^{206}\text{Pb}/^{238}\text{U}$		$^{208}\text{Pb}/^{232}\text{Th}$		
	Bias Corr.	2%SD	Bias Corr.	2%SD	Bias Corr.	2%SD	rho	Bias Corr.	2%SD
Zircon 26	0.1365	34.5005	0.0175	32.2333	0.0008	11.6370	0.0212	0.0005	18.1863
Zircon 27	0.0721	28.9985	0.0355	27.7946	0.0034	8.7471	0.0167	0.0018	21.0308
Zircon 27-2	0.0602	25.0122	0.0256	25.2383	0.0037	6.8561	0.1687	0.0014	12.8085
Zircon 28	0.0551	9.6854	0.0842	10.0323	0.0114	5.3396	0.3300	0.0036	10.7877
Zircon 29	0.0636	13.1147	0.0545	12.1545	0.0066	5.9693	0.0784	0.0025	10.3807
Zircon 30	0.1721	1.7050	7.6319	5.3517	0.3224	5.3676	0.9494	0.1214	4.2525
Zircon 31	0.0956	1.4813	3.0141	4.4207	0.2268	4.5570	0.9460	0.0681	4.4434
Zircon 32-1	0.0480	5.0812	0.0663	6.5676	0.0100	5.0203	0.6448	0.0030	5.7729
Zircon 32-2	0.0492	3.7554	0.0640	5.3143	0.0095	4.7040	0.7254	0.0029	5.0011
Zircon 33	0.0508	8.3370	0.0301	8.8599	0.0044	5.1327	0.3885	0.0014	7.5887
Zircon 34	0.1032	1.9169	2.8719	4.9989	0.2021	5.1017	0.9282	0.0717	4.6839
Zircon 35-1	0.0834	2.0796	1.3314	7.3038	0.1163	7.2066	0.9590	0.0464	14.6829
Zircon35-2	0.0924	1.6141	2.6663	4.4319	0.2075	4.5990	0.9368	0.0603	5.1574
Zircon 36	0.0526	6.5353	0.1199	6.8730	0.0164	5.0352	0.4317	0.0044	8.6228
Zircon 37-1	0.1363	25.3815	0.0153	22.6451	0.0007	10.7618	0.0320	0.0003	15.3190
Zircon 37-2	0.3071	12.2767	0.0452	10.1752	0.0010	9.6408	0.2333	0.0009	11.4628
Zircon 37-3	0.1039	29.6306	0.0084	31.6311	0.0007	9.8640	0.3523	0.0003	17.2310
Zircon 38	0.1002	1.7844	3.6089	4.5918	0.2618	4.7501	0.9276	0.0743	4.3238
Zircon 39	0.0676	11.4849	0.0060	10.9834	0.0007	5.9617	0.1854	0.0002	5.7020
Zircon 40	0.0953	2.0528	2.3112	5.3193	0.1731	5.3810	0.9265	0.0572	7.5441
Zircon 41	0.0784	23.0901	0.0056	15.0442	0.0007	6.1980	0.8000	0.0002	9.0174
Zircon 42	0.0860	45.8340	0.0068	56.0977	0.0007	11.6527	0.9041	0.0004	31.9178
Zircon 43	0.0491	3.1712	0.1435	5.2107	0.0212	4.6561	0.7991	0.0071	4.8440
Zircon 44-1	0.0550	42.8629	0.0054	45.2830	0.0006	18.3746	0.3311	0.0002	18.5436
Zircon 44-2	0.0863	27.9627	0.0080	28.2051	0.0007	16.5663	0.3082	0.0002	16.7536
Zircon 45	0.1376	23.1040	0.0151	19.5946	0.0007	17.9884	0.2465	0.0004	18.1611
Zircon 46-1	0.0900	1.6667	2.6704	2.1772	0.2139	3.3835	0.9102	0.0782	4.2059
Zircon 46-2	0.0907	1.6538	2.7071	1.8086	0.2160	2.7829	0.8226	0.0792	3.7399
Zircon 47	0.0493	8.9249	0.0748	8.4584	0.0106	7.6233	0.3877	0.0033	8.0223

Table 4: Zircon LA-ICP-MS Apparent age data

Data	$^{206}\text{Pb}/^{238}\text{U}$		$^{207}\text{Pb}/^{235}\text{U}$		$^{207}\text{Pb}/^{206}\text{Pb}$		$^{208}\text{Pb}/^{232}\text{Th}$	
	Age	2SD	Age	2SD	Age	2SD	Age	2SD
Zircon 1	90.20	4.5082	90.88	5.1271	57.40	107.4847	96.60	6.7089
Zircon 2	91.53	4.6239	95.78	6.3011	211.48	120.6733	98.74	5.8440
Zircon 3-1	6.60	0.4883	6.19	1.9381	49.05	531.0237	10.47	2.2011
Zircon 3-2	6.38	0.3580	7.05	0.7988	165.55	246.1755	5.99	0.7370
Zircon 3-3	6.64	0.4721	5.87	1.6310	189.22	884.3838	5.66	1.4094
Zircon 4-1	1777.40	76.6051	1760.70	40.9074	1755.24	30.7200	1864.08	85.1810
Zircon 4-2	1698.97	81.5741	1701.03	44.9279	1694.65	33.3623	1799.85	85.8834
Zircon 5	66.98	3.4311	71.61	6.1916	276.48	190.5930	65.47	7.3449
Zircon 6-1	76.78	3.6162	75.29	3.8602	19.14	79.7078	73.31	5.5585
Zircon 6-2	330.23	26.4604	524.68	37.8590	1409.33	55.5686	466.48	42.5423
Zircon 6-3	570.28	29.3803	838.27	30.8364	1598.77	33.5464	741.46	37.4210
Zircon 7-1	4.61	0.4736	7.23	3.5631	309.86	1340.0410	4.70	1.7906
Zircon 7-2	4.16	0.4956	4.45	3.6589	751.54	1303.9923	5.50	2.1128
Zircon 7-3	4.31	0.5088	5.73	4.6350	1129.61	1106.2518	2.58	2.5848
Zircon 7-4	3.95	0.4972	3.06	4.3404	515.61	1633.1825	5.80	3.0709
Zircon 7-5	5.22	0.5596	2.55	3.8277	5087.65	2356.5866	4.33	2.0914
Zircon 8-1	1251.90	73.1157	1440.01	50.9564	1705.89	31.6079	1208.28	85.1304
Zircon 8-2	646.79	51.5305	904.62	53.9742	1528.77	51.6471	915.42	85.8913
Zircon 9-1	1213.74	50.8212	1327.11	32.7906	1506.97	31.7591	1451.39	64.9044
Zircon 9-2	1701.89	72.0564	1637.76	38.1418	1540.89	36.4834	1631.00	78.4625
Zircon 10-1	93.44	8.7480	98.88	14.5925	113.42	230.3457	76.55	5.7691
Zircon 10-2	71.58	3.7105	72.22	6.1660	128.54	194.5298	72.78	4.7620
Zircon 11	1347.81	55.5782	1408.15	33.9568	1492.12	30.2490	1403.96	58.0507
Zircon 12	1319.43	56.6719	1340.52	35.8098	1367.47	36.3276	1270.69	55.3189
Zircon 13	1069.17	55.8384	1150.74	39.5265	1349.87	38.7414	1209.96	52.6264
Zircon 14	7.25	0.5877	9.60	2.7690	574.93	628.8724	3.91	2.3504
Zircon 15-1	67.95	3.4302	74.89	6.2114	295.50	175.8064	71.38	4.3340
Zircon 15-2	72.18	3.9753	79.52	8.3297	393.24	247.5841	75.17	6.9001
Zircon 16	4.99	0.6913	28.35	8.1057	2887.60	444.1958	17.12	3.4897
Zircon 17-1	71.14	3.3364	79.09	4.7911	317.81	113.5535	82.36	6.4689
Zircon 17-2	66.53	3.1106	71.85	3.8999	283.56	89.9334	67.32	3.4456
Zircon 18-1	6.06	0.6986	16.01	5.2122	1817.61	646.5840	12.51	2.8235
Zircon 18-2	7.77	0.7249	19.30	4.5685	1998.50	437.3308	16.35	3.3026
Zircon 19	50.40	2.4260	50.58	2.9183	52.47	103.2522	45.24	3.6985
Zircon 20	100.21	8.0769	133.50	14.0222	628.16	122.0663	309.90	47.1355
Zircon 21	91.83	4.2423	93.22	4.7619	103.35	85.7331	86.16	4.6962
Zircon 22	4.12	0.3937	5.06	2.2112	770.76	806.9960	3.83	0.6150
Zircon 22-2	3.95	0.3381	4.50	1.7498	1364.23	797.1001	4.61	0.5503
Zircon 23	1480.31	65.7875	1556.20	37.7401	1651.85	32.6514	1543.44	64.6839
Zircon 24-1	23.43	1.5900	46.15	6.1344	1803.30	330.9558	38.13	5.3807
Zircon 24-2	25.66	1.4290	26.74	3.4355	347.21	297.5370	25.09	2.6165
Zircon 25	4.36	0.3518	7.57	1.6441	1387.40	480.1894	4.14	0.4400

Table 4 continued: Zircon LA-ICP-MS apparent age data

Data		$^{206}\text{Pb}/^{238}\text{U}$		$^{207}\text{Pb}/^{235}\text{U}$		$^{207}\text{Pb}/^{206}\text{Pb}$		$^{208}\text{Pb}/^{232}\text{Th}$	
Analysis_#	Age	2SD	Age	2SD	Age	2SD	Age	2SD	
Zircon 26	4.98	0.5791	17.61	5.6282	2182.92	600.3409	9.35	1.7001	
Zircon 27	22.08	1.9276	35.37	9.6621	987.96	589.9957	37.18	7.8138	
Zircon 27-2	23.72	1.6232	25.61	6.3838	609.67	540.6582	28.42	3.6378	
Zircon 28	72.84	3.8674	82.06	7.9085	415.75	216.4144	72.82	7.8432	
Zircon 29	42.17	2.5093	53.81	6.3702	729.04	277.9559	49.71	5.1550	
Zircon 30	1802.86	84.4315	2186.76	48.0401	2578.26	28.4798	2316.76	93.2989	
Zircon 31	1318.98	54.3609	1409.98	33.6880	1540.84	27.8548	1332.05	57.3620	
Zircon 32-1	64.17	3.2056	65.14	4.1437	98.33	120.2325	60.45	3.4848	
Zircon 32-2	60.96	2.8541	62.96	3.2441	157.32	87.8953	58.90	2.9414	
Zircon 33	28.11	1.4398	30.14	2.6307	232.19	192.4743	27.45	2.0817	
Zircon 34	1187.65	55.3423	1373.39	37.6338	1683.04	35.3883	1399.15	63.4169	
Zircon 35-1	709.75	48.4366	858.77	42.3403	1277.61	40.5424	917.34	132.1118	
Zircon35-2	1216.59	50.9933	1318.04	32.7098	1475.71	30.6174	1183.22	59.3585	
Zircon 36	105.06	5.2471	114.88	7.4652	313.54	148.6859	88.08	7.5799	
Zircon 37-1	4.67	0.5021	15.38	3.4576	2180.63	441.7713	6.24	0.9552	
Zircon 37-2	6.71	0.6466	44.87	4.4662	3506.52	189.6646	17.69	2.0272	
Zircon 37-3	4.20	0.4142	8.51	2.6799	1695.75	546.1319	5.14	0.8861	
Zircon 38	1500.23	63.5855	1550.18	36.4930	1627.84	33.1756	1448.97	60.5478	
Zircon 39	4.33	0.2583	6.11	0.6686	855.26	238.5362	4.29	0.2443	
Zircon 40	1030.30	51.2412	1214.69	37.6847	1534.47	38.6338	1124.95	82.7171	
Zircon 41	4.23	0.2624	5.63	0.8443	1157.98	457.9824	4.84	0.4366	
Zircon 42	4.32	0.5028	6.83	3.8175	1337.30	886.0716	8.69	2.7735	
Zircon 43	135.48	6.2420	136.03	6.6336	151.71	74.2997	142.22	6.8663	
Zircon 44-1	4.17	0.7656	5.47	2.4702	413.68	958.0904	4.20	0.7795	
Zircon 44-2	4.36	0.7224	8.04	2.2586	1345.17	539.9854	4.93	0.8261	
Zircon 45	4.62	0.8310	15.2	2.9563	2197.40	401.3933	7.68	1.3944	
Zircon 46-1	1250.43	38.4611	1319	16.0717	1425.53	31.8302	1521.91	61.7546	
Zircon 46-2	1261.64	31.8913	1329	13.3997	1440.31	31.5210	1541.19	55.5729	
Zircon 47	68.18	5.1699	73.1	5.9696	162.12	208.7044	66.15	5.2987	

Table 5: Zircon LA-ICP-MS data included in youngest cluster of grains

Data									
Analysis_#	$^{207}\text{Pb}/^{206}\text{Pb}$	2%SD	$^{207}\text{Pb}/^{235}\text{U}$	2%SD	$^{206}\text{Pb}/^{238}\text{U}$	2%SD	rho	$^{208}\text{Pb}/^{232}\text{Th}$	2%SD
Zircon 7-1	0.0526	58.8609	0.0071	49.4799	0.0007	10.2872	0.8944	0.0002	38.1409
Zircon 7-2	0.0643	61.7510	0.0044	82.3212	0.0006	11.9030	0.8000	0.0003	38.4435
Zircon 7-3	0.0773	55.5418	0.0057	81.1349	0.0007	11.7945	0.8000	0.0001	100.0798
Zircon 7-4	0.0576	74.3631	0.0030	141.9928	0.0006	12.5878	0.8000	0.0003	52.9288
Zircon 16	0.2077	27.3655	0.0283	28.9951	0.0008	13.8698	0.3534	0.0008	20.3952
Zircon 22	0.0649	38.3344	0.0050	43.8226	0.0006	9.5705	0.6467	0.0002	16.0434
Zircon 22-2	0.0872	41.3867	0.0044	38.9850	0.0006	8.5622	0.1793	0.0002	11.9463
Zircon 25	0.0882	25.0122	0.0075	21.8053	0.0007	8.0768	0.2410	0.0002	10.6333
Zircon 26	0.1365	34.5005	0.0175	32.2333	0.0008	11.6370	0.0212	0.0005	18.1863
Zircon 37	0.1363	25.3815	0.0153	22.6451	0.0007	10.7618	0.0320	0.0003	15.3190
Zircon 37-2	0.3071	12.2767	0.0452	10.1752	0.0010	9.6408	0.2333	0.0009	11.4628
Zircon 37-3	0.1039	29.6306	0.0084	31.6311	0.0007	9.8640	0.3523	0.0003	17.2310
Zircon 39	0.0676	11.4849	0.0060	10.9834	0.0007	5.9617	0.1854	0.0002	5.7020
Zircon 41	0.0784	23.0901	0.0056	15.0442	0.0007	6.1980	0.8000	0.0002	9.0174
Zircon 42	0.0860	45.8340	0.0068	56.0977	0.0007	11.6527	0.9041	0.0004	31.9178
Zircon 44-1	0.0550	42.8629	0.0054	45.2830	0.0006	18.3746	0.3311	0.0002	18.5436
Zircon 44-2	0.0863	27.9627	0.0080	28.2051	0.0007	16.5663	0.3082	0.0002	16.7536
Zircon 45	0.1376	23.1040	0.0151	19.5946	0.0007	17.9884	0.2465	0.0004	18.1611

Table 6: Zircon LA-ICP-MS apparent age data included in youngest cluster of grains

Analysis #	$^{206}\text{Pb}/^{238}\text{U}$		$^{207}\text{Pb}/^{235}\text{U}$		$^{207}\text{Pb}/^{206}\text{Pb}$		$^{208}\text{Pb}/^{232}\text{Th}$	
	Age	2SD	Age	2SD	Age	2SD	Age	2SD
Zircon 7-1	4.61	0.4736	7.23	3.5631	309.86	1340.0410	4.70	1.7906
Zircon 7-2	4.16	0.4956	4.45	3.6589	751.54	1303.9923	5.50	2.1128
Zircon 7-3	4.31	0.5088	5.73	4.6350	1129.61	1106.2518	2.58	2.5848
Zircon 7-4	3.95	0.4972	3.06	4.3404	515.61	1633.1825	5.80	3.0709
Zircon 16	4.99	0.6913	28.35	8.1057	2887.60	444.1958	17.12	3.4897
Zircon 22	4.12	0.3937	5.06	2.2112	770.76	806.9960	3.83	0.6150
Zircon 22-2	3.95	0.3381	4.50	1.7498	1364.23	797.1001	4.61	0.5503
Zircon 25	4.36	0.3518	7.57	1.6441	1387.40	480.1894	4.14	0.4400
Zircon 26	4.98	0.5791	17.61	5.6282	2182.92	600.3409	9.35	1.7001
Zircon 37	4.67	0.5021	15.38	3.4576	2180.63	441.7713	6.24	0.9552
Zircon 37-2	6.71	0.6466	44.87	4.4662	3506.52	189.6646	17.69	2.0272
Zircon 37-3	4.20	0.4142	8.51	2.6799	1695.75	546.1319	5.14	0.8861
Zircon 39	4.33	0.2583	6.11	0.6686	855.26	238.5362	4.29	0.2443
Zircon 41	4.23	0.2624	5.63	0.8443	1157.98	457.9824	4.84	0.4366
Zircon 42	4.32	0.5028	6.83	3.8175	1337.30	886.0716	8.69	2.7735
Zircon 44-1	4.17	0.7656	5.47	2.4702	414	958.0904	4.20	0.7795
Zircon 44-2	4.36	0.7224	8.04	2.2586	1345	539.9854	4.93	0.8261
Zircon 45	4.62	0.8310	15.2	2.9563	2197	401.3933	7.68	1.3944

Bibliography

- Andersen, T. (2002) Correction of Common Lead in U–Pb Analyses That Do Not Report 204Pb. *Chemical Geology*, 192(1), 59–79.
- Bender, A.M. et al. (2016) Differential Uplift and Incision of the Yakima River Terraces, Central Washington State. *Journal of Geophysical Research. Solid Earth*, 121(1), 365–384.
- Bolte, T. et al. (2015) The Blacktail Creek Tuff: An Analytical and Experimental Study of Rhyolites from the Heise Volcanic Field, Yellowstone Hotspot System. *Contributions to Mineralogy and Petrology*, 169(2), 1837–.
- Bretz, J.H. et al. (1956) Channeled Scabland of Washington: New Data and Interpretations. *Geological Society of America Bulletin*, 67(8), 957–1049.
- Chew, D.M. et al. (2014) U-Pb LA-ICPMS Dating Using Accessory Mineral Standards with Variable Common Pb. *Chemical Geology*. 363, 185–199.
- Chew, D. et al. (2019) Ultrafast, > 50 Hz LA-ICP-MS Spot Analysis Applied to U-Pb Dating of Zircon and Other U-Bearing Minerals. *Geostandards and Geoanalytical Research*, 43(1), 39–60
- Dickinson, & Gehrels, G. E. (2009) Use of U-Pb Ages of Detrital Zircons to Infer Maximum Depositional Ages of Strata; A Test Against a Colorado Plateau Mesozoic Database. *Earth and Planetary Science Letters*, 288 (1-2), 115–125.
- Emery-Wetherell, M., & Schilter, J. (2020) A New Early Occurrence of Cervidae in North America from the Miocene-Pliocene Ellensburg Formation in Washington, USA. *Palaeontologia Electronica*, 23(1)
- Erikson, E.H. (1977) Petrology and Petrogenesis of the Mount Stuart Batholith; Plutonic Equivalent of the High-Alumina Basalt Association? *Contributions to Mineralogy and Petrology*, 60(2), 183–207.
- Gunnell, & Foral, A. (1994) New Species of *Bretzia* (Cervidae; Artiodactyla) from the Latest Pleistocene or Earliest Holocene of Nebraska and South Dakota. *Journal of Mammalogy*, 75(2), 378–381.
- Gustafson, E.P. (2015) An Early Pliocene North American Deer: *Bretzia Pseudalces*, its Osteology, Biology, and Place in Cervid History. *Bulletin of the Museum of Natural History, University of Oregon*, 25, 1-75.
- Krummenacher, D. (1970) Isotopic Composition of Argon in Modern Surface Volcanic Rocks. *Earth and Planetary Science Letters*, 8(2), 109–11.
- Jicha, B.R. et al. (2009) Isotopic and Trace Element Constraints on the Petrogenesis of Lavas from the Mount Adams Volcanic Field, Washington. *Contributions to Mineralogy and Petrology*, 157(2), 189–207.
- Kelley, S. (2002) K-Ar and Ar-Ar Dating. *Reviews in Mineralogy and Geochemistry*, 47(1), 785–818.
- Lamb, J. (1997) Quaternary Stratigraphy of the Kittitas Valley with Emphasis on the Craigs Hill Section. *Senior Undergraduate Thesis, Central Washington University*, 1-109.
- Lapen, T.J. et al. (2017) Two billion Years of Magmatism Recorded from a Single Mars Meteorite Ejection Site. *Science Advances*, 3(2), e1600922–e1600922.
- Lapen, T.J. et al. (2004) High Precision Lu and Hf Isotope Analyses of Both Spiked and Unspiked Samples; A New Approach. *Geochemistry, Geophysics, Geosystems:G3*, 5(1), Q01010–n/a.
- Ludwig, K. (1998) On the Treatment of Concordant Uranium-Lead Ages. *Geochimica et Cosmochimica Acta*, 62(4), 665–676.
- Ludwig, K. (2000) Users Manual for Isoplot/Ex: A Geochronological Toolkit for Microsoft Excel. *Berkeley Geochronology Center Special Publications*, 1a. 53.

- Martin, J.E. & Mallory, V.S. (2011) Vertebrate Paleontology of the Late Miocene (Hemphillian) Wilbur Locality of Central Washington. *Paludicola*, 8, 155-185.
- Matzel, J.E.P. et al. (2006) Time Scales of Pluton Construction at Differing Crustal Levels; Examples from the Mount Stuart and Tenpeak Intrusions, North Cascades, Washington. *Geological Society of America Bulletin*, 118(11-12), 1412–1430.
- Miller, J.S. et al. (2007) Zircon Growth and Recycling During the Assembly of Large, Composite Arc Plutons. *Journal of Volcanology and Geothermal Research*, 167(1-4), 282–299.
- Nash, B.P. et al. (2006) The Yellowstone Hotspot in Space and Time; Nd and Hf Isotopes in Silicic Magmas. *Earth and Planetary Science Letters*, 247(1-2), 143–156.
- O'Sullivan, G. et al. (2020) The Trace Element Composition of Apatite and Its Application to Detrital Provenance Studies. *Earth-Science Reviews*, 201, 103044.
- Parrish, & Noble, S. R. (2003) Zircon U-Th-Pb Geochronology by Isotope Dilution; Thermal Ionization Mass Spectrometry (ID-TIMS). *Reviews in Mineralogy and Geochemistry*, 53(1), 183–213.
- Reidel, S. P. et al. (2013) The Columbia River Flood Basalt Province; Stratigraphy, Areal Extent, Volume, and Physical Volcanology, *In Special Paper - Geological Society of America*, 497, 1–43.
- Reidel, S.P. & Tolan, T. L. (2013) The Late Cenozoic Evolution of the Columbia River System in the Columbia River Flood Basalt Province. *In Special Paper - Geological Society of America*, 497, 201-230
- Sadowski, A.J. et al. (2020) Geologic map of the Ellensburg North and Southern Half of the Reecer Canyon 7.5-Minute Quadrangles, Kittitas County, Washington: *Washington Geological Survey Map Series 2020-01*, 1 sheet, scale 1:24,000, 25 p. text.
- Schaen, A.J. et al. (2021) Interpreting and Reporting $^{40}\text{Ar}/^{39}\text{Ar}$ Geochronologic Data. *Geological Society of America Bulletin*, 133(3-4), 461–487.
- Shaulis, B. et al. (2010) Signal Linearity of an Extended Range Pulse Counting Detector; Applications to Accurate and Precise U-Pb Dating of Zircon by Laser Ablation Quadrupole ICP-MS. *Geochemistry, Geophysics, Geosystems*: G3. [Online] 11(11), np–n/a.
- Sherrod D.R. & Smith, J.G. (1990) Quaternary Extrusion rates of the Cascade Range, Northwestern United States and Southern British Columbia. *Journal of Geophysical Research*, 95(B12), 19465–19474.
- Slama, J., et al. (2008) Plesovice Zircon; A New Natural Reference Material for U/Pb and Hf Isotopic Microanalysis. *Chemical Geology*, 249(1-2), 1–35.
- Smith, G.A. et al. (1988) Eruptive Style and Location of Volcanic Centers in the Miocene Washington Cascade Range; Reconstruction from the Sedimentary Record." *Geology (Boulder)*, 16(4), 337–340.
- Smith, G.A. (1988) Neogene Synvolcanic and Syntectonic Sedimentation in Central Washington. *Geological Society of America Bulletin*, 100(9), 1479–1492.
- Smith, G.A. (1988). Sedimentology of Proximal to Distal Volcaniclastics Dispersed Across an Active Foldbelt: Ellensburg Formation (Late Miocene), Central Washington. *Sedimentology*, 35, 953-977.
- Smith, G.A. et al. (1989) Geochronology of the Ellensburg Formation-Constraints on Neogene Volcanism and Stratigraphic Relationships in Central Washington. *Isochron/West, Bulletin of Isotopic Geochronology*, 53, 28–32.
- Spencer, C.J. et al. (2016) Strategies Towards Statistically Robust Interpretations of in Situ U–Pb Zircon Geochronology. *Di Xue Qian Yuan.*, 7(4), 581–89.
- Stern, R.J. & Dumitru, T.A. (2019) Eocene Initiation of the Cascadia Subduction Zone; a Second Example of Plume-Induced Subduction Initiation? *Geosphere*, 15(3) 659–81.

- Tera, & Wasserburg, G. J. (1972) U-Th-Pb Systematics in Three Apollo 14 Basalts and the Problem of Initial Pb in Lunar Rocks. *Earth and Planetary Science Letters*, 14 (3), 281–304.
- Waitt, R.B. (1979) *Late Cenozoic Deposits, Landforms, Stratigraphy, and Tectonism in Kittitas Valley, Washington*. Department of the Interior, Geological Survey.
- Watts, K. E. et al. (2011) Large-Volume Rhyolite Genesis in Caldera Complexes of the Snake River Plain; Insights from the Kilgore Tuff of the Heise Volcanic Field, Idaho, with Comparison to Yellowstone and Bruneau-Jarbidge Rhyolites. *Journal of Petrology*, 52 (5), 857–90.
- Wetherill, G.W. (1956) Discordant Uranium-Lead Ages, I. *Eos, Transactions American Geophysical Union*, 37(3), 320–326.
- Zi, Jian-Wei, et al. (2022) In Situ U-Pb and Geochemical Evidence for Ancient Pb-Loss During Hydrothermal Alteration Producing Apparent Young Concordant Zircon Dates in Older Tuffs. *Geochimica et Cosmochimica Acta*, 320, 324–338